The Thesis Committee for Somnath Mondal
Certifies that this is the approved version of the following thesis:

Pressure Transients in Wellbores: Water Hammer Effects and Implications for Fracture Diagnostics

APPROVED BY
SUPERVISING COMMITTEE:

Supervisor:

Mukul M. Sharma

David DiCarlo

Pressure Transients in Wellbores: Water Hammer Effects and Implications for Fracture Diagnostics

by

Somnath Mondal, B.E.

Thesis

Presented to the Faculty of the Graduate School of

The University of Texas at Austin

in Partial Fulfillment

of the Requirements

for the Degree of

Master of Science in Engineering

The University of Texas at Austin

December, 2010

Dedication

To my family and friends.

Acknowledgements

It is a pleasure to thank those who made this thesis possible. I owe my deepest gratitude to my supervisor, Dr. Mukul M. Sharma, for his constant encouragement, guidance and support over the past two years. I would like to thank Dr. David DiCarlo for taking time to read and review this work.

I would like to thank the members of the Hydraulic Fracturing and Sand Control Joint Industry Project (JIP) at the University of Texas for their financial support. I would like to specifically thank Mr. Adi Venkitaraman of Chevron for providing field data. I also express my sincere gratitude to Dr. George Wong of Shell for his expertise that has been immensely helpful in formulating this problem, and also for providing field data.

I would like to acknowledge Jin Lee for her support in maintaining this wonderful research group. I thank my family and friends for making me who I am.

December, 2010

Abstract

Pressure Transients in Wellbores: Water Hammer Effects and Implications for Fracture Diagnostics

Somnath Mondal, MSE

The University of Texas at Austin, 2010

Supervisor: Mukul M. Sharma

A pressure transient is generated when a sudden change in injection rate occurs due to a valve closure or injector shutdown. This pressure transient, referred to as a water hammer, travels down the wellbore, is reflected back and induces a series of pressure pulses on the sand face. This study presents a semi-analytical model to simulate the magnitude, frequency and duration of water hammer in wellbores. An impedance model has been suggested that can describe the interface, between the wellbore and the formation. Pressure transients measured in five wells in an offshore field are history matched to validate the model. It is shown that the amplitude of the pressure waves may be up to an order of magnitude smaller at the sand face when compared with surface measurements. Finally, a model has been proposed to estimate fracture dimensions from water hammer data.

Table of Contents

List of Tables

List of Figures

Chapter 1: Introduction

A change in flow causes a change in pressure, and vice-versa, which leads to transients in hydraulic systems. Water hammer is a surge or pressure wave that is created due to a sudden change in flow velocity in a confined system. It is a transient phenomenon that may be triggered by abrupt opening or closing of valves, starting or stopping of pumps, failure of mechanical devices in a flow line, etc. The name, water hammer, originates from the hammering sound that sometimes accompanies this phenomenon (Parmakian, 1963). The variation in pressure due to water hammer can be large, sometimes in the order of thousands of psi. The pressure fluctuations then propagate in the system like a wave and may cause severe damage.

A conceptual schematic of water hammer in a simple system is shown in Fig. 1.1. The system consists of a frictionless horizontal pipe of constant diameter, which is fed by a reservoir at constant pressure, and is connected to a downstream valve that is suddenly closed.

1. At $t = 0$, the pressure head is steady down the length of the pipe, as shown by the constant hydraulic grade line (shown in red), because friction was neglected, and the flow velocity is v_0.
2. As soon as the valve is shut-in, the fluid element closest to the valve comes to rest, and this rate of change of momentum causes a rise in the pressure head by $+\Delta H$. As subsequent fluid elements come to rest, the high pressure propagates upstream from the valve towards the reservoir like a pressure wave.
3. At $t = L/a$, where L is the pipe length and a is the wave speed, the high-pressure wave reaches the reservoir as all the fluid in the pipe comes to

rest. However, this causes a pressure discontinuity at the boundary with the constant pressure reservoir.

4. In order to achieve pressure equilibrium at the reservoir, a pressure wave of magnitude $-\Delta H$ is reflected back towards the valve and the direction of the flow velocity reverses towards the reservoir. This reflected wave reaches the downstream valve at $t = 2L/a$. This time is called the *reflection time*, T_r.
5. At $t = 2L/a$, the flow velocity in the entire pipe is $-v_0$. This causes another discontinuity at the downstream valve, where the velocity must be zero.
6. The change in velocity from $-v_0$ to zero, cause a sudden negative change in pressure of $-\Delta H$. This low-pressure wave travels upward as the fluid in the pipe again comes to rest, reaching the reservoir at $t = 1.5T_r$.
7. At $t = 1.5T_r$, the fluid in the pipe is at rest but there is a discontinuity at the constant pressure reservoir boundary.
8. As the pressure resumes the reservoir pressure, a wave of increased pressure originating from the reservoir travels back to the valve as the flow velocity in the pipe changes to v_0.
9. At $t = 2T_r$, the conditions in the system are the same as 1, and the whole process starts over again.

Some of the earliest studies and experiments in water hammer were done by Joukowsky (1900). The Joukowsky equation states that the rise in peizometric head (ΔH) due to the fast shut-in of a downstream valve ($T_c < 2L/a$) is given by:

$$\Delta H = \frac{a V_0}{g} \tag{1.1}$$

where a is the pressure wave-speed, V_0 the initial flow velocity, g the acceleration due to gravity, L the pipe length, and T_c the valve closure time. The time period, $2L/a$, is the time taken by the pressure wave to propagate down the pipe length, get reflected and travel back. It is essential to consider the peak pressures due to water hammer in the design of any pipeline system, which makes water hammer a well-studied topic in civil engineering. Various researchers have simulated transient flow in pipeline systems with different methods, a discussion of which follows in the next section.

Water hammer is a fast transient in the wellbore as compared to the conventional pressure transient response of the reservoir. Water hammer, in the upstream petroleum industry, has been a largely under-studied phenomenon. However, it has been a known issue following emergency shut-ins of water injectors. Due to safety concerns, the number of emergency shut downs of offshore injection wells can be high, with more than 80 emergency shut downs per year in some cases (McCarty and Norman, 2006). In recent years, with the increasing number of offshore water injectors, it has been observed that injection wells that undergo repeated shut-ins show reduced injectivity, higher sand production and even failure of downhole completion (Vaziri et al., 2007). This observation has been widely attributed to the cyclic pressure waves induced by water hammer (Santarelli et al., 2000; Hayatdavoudi, 2006; McCarty and Norman, 2006; Vaziri et al., 2007; Wang et al., 2008). It is believed that in weak sands, pressure fluctuations as low as tens of psi, at the sand face, might be sufficient to cause sand failure (Santarelli et al., 2000). Modeling work by Vaziri et al. (2007) have also shown that cyclic pressure fluctuations cause more sanding than a monotonic increase in injection pressure.

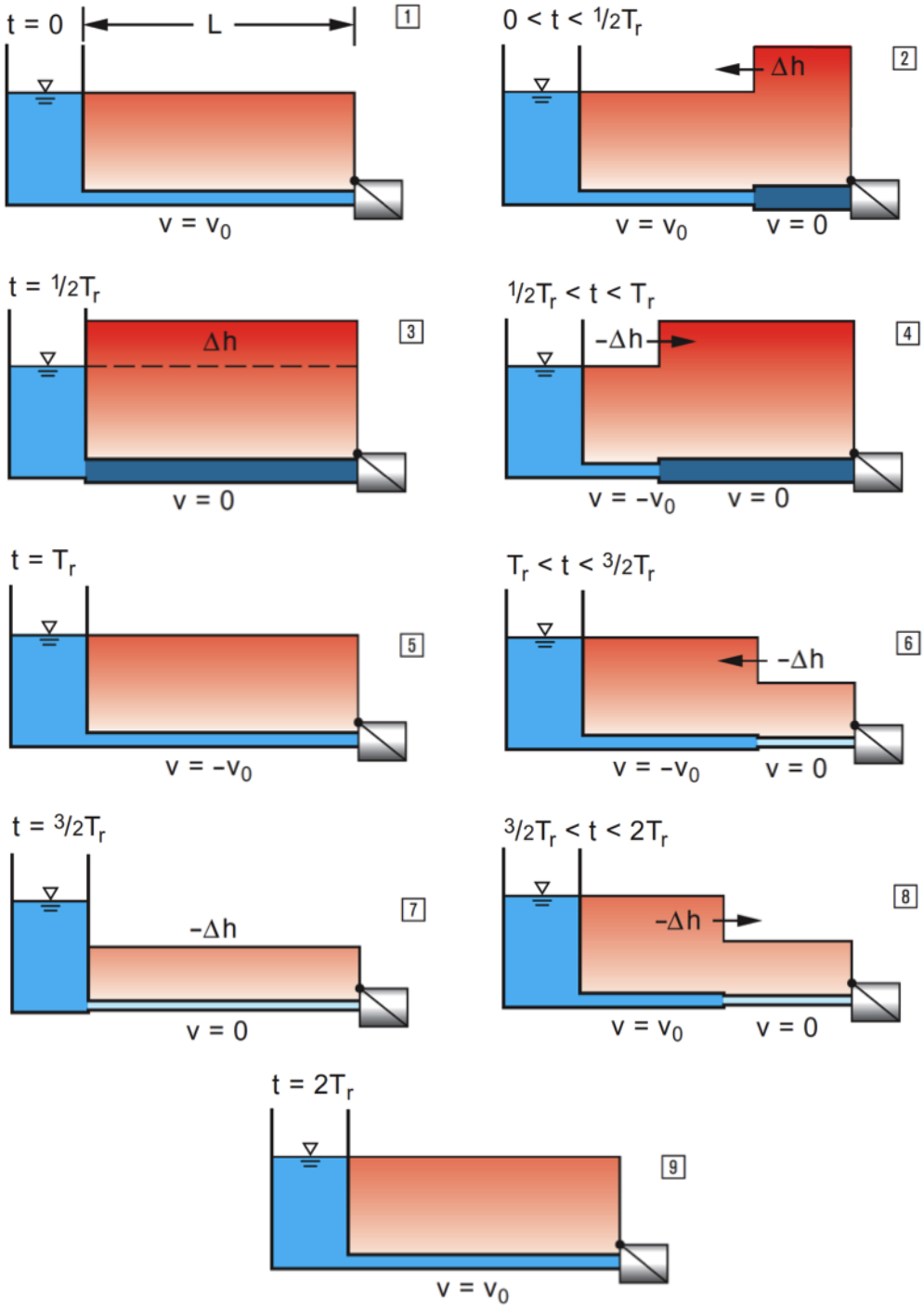

Figure 1.1: Conceptual schematic of water hammer in a reservoir-pipe-valve system (From KSB Know-how series on Water Hammer)

The magnitude of water hammer measured at the wellhead is often in the order of hundreds of psi, however, there is almost no bottomhole water hammer pressure data in injectors to confirm the magnitude at the sand face. It is, therefore, important to model water hammer in injectors. The first objective of this study is to model water hammer in injectors in order to estimate bottomhole water hammer pressures from measured surface data.

It is also well known that sonic waves can be used to determine important information about fracture and formation properties (Mathieu, 1984; Medlin, 1991). In fact, it has been proved that fracture dimensions can be estimated from the propagation and reflection of a single pressure pulse induced at the surface of a wellbore (Holzhausen and Gooch, 1985; Paige et al., 1992). In principle therefore, it should also be possible to extract similar information from the analysis of water hammer pressure waves. Moreover, there is almost always a pressure gauge at the wellhead and water hammer pressure data can be collected without any extra effort. Hence, any information that can be derived from this data, independent of conventional testing methods, could be attractive and useful to the oil industry. The second objective of this study is to develop a model to estimate fracture connectivity and/or dimensions from water hammer pressure data.

1.1 LITERATURE REVIEW

1.1.1 Water hammer Modeling

Classical solutions of the basic unsteady flow equations were developed by Allievi (1902, 1913) by analytical and graphical methods after neglecting the friction terms. Bergeron (1935, 1936) also developed graphical solutions that were used popularly before the advent of computers. Friction could be included by complex procedures and for practical reasons the analysis was limited to single pipelines. Streeter

and Wylie (1967) proposed and popularized the explicit method of characteristics (MOC) to solve the water hammer equations. Shimada and Okushima (1984) solved the water hammer equations by a series solution method and a Newton-Rhapson method. Chaudhry and Hussaini (1985) used MacCormak, Lambda and Gabutti Finite Difference (FD) schemes to numerically solve the water hammer equations. Izquierdo and Iglesias (2002, 2004) developed a computer program using method of characteristics to simulate transients in simple and complex pipeline systems. Silva-Araya and Chaudhury (1997) solved the hyperbolic part of the equations in one-dimensional form by MOC and the parabolic part in quasi-two-dimensional using finite difference. Ghidaoui et al. (2002) proposed a two-layer and five-layer eddy viscosity model for water hammer where a dimensionless parameter (the ratio of the time scale of the radial diffusion of shear to the time scale of wave propagation) was used to estimate the accuracy of the assumption of flow axisymmetry. Zhao and Ghidaoui (2003) have solved a model for quasi-two-dimensional turbulent water hammer flow. Zhao and Ghidaoui (2004) have also developed first and second-order Godunov-type explicit finite volume (FV) schemes for water hammer problems. They have compared their schemes with MOC considering space-line interpolation for three test cases with and without friction. They found that the first-order FV schemes have the same accuracy as MOC with space-line interpolation but for a given level of accuracy, the second-order scheme requires much less memory and execution time than the first-order Godunov-type scheme. Wood (2005a, 2005b) proposed the Wave Characteristic Method (WCM) and demonstrated that though, both WCM and MOC, have the same level of accuracy, the WCM is more computationally efficient for complex pipe systems. Greyvenstein (2006) proposed an implicit FD method based on the simultaneous pressure correction approach. Afshar and Rohani (2008) proposed a water hammer simulation using an implicit MOC scheme. It is evident from a

study of the previous work done that there are various numerical models such as explicit and implicit Method of Characteristics, explicit and implicit finite difference, finite volume and finite element to solve hydraulic transient problems. Among these methods, the explicit MOC is the most popular for water hammer simulations for being simple to code, accurate and efficient.

The general way of calculating friction losses in transient flows were using formulae developed for steady-state conditions, for example the use of Darcy-Weisbach equation for friction based on the mean flow velocity assumes that the shear stress at the wall is the same for steady-state and transient flow conditions. The MOC solutions were improved by incorporating unsteady or transient friction models instead of constant or steady state friction used in the early models. Zielke (1968) proposed a convolution based frequency dependepent model of unsteady friction for laminar flows that was very computationally intensive. Trikha (1975) improved the computation speed of Zielke's model by using approximate expressions for Zielke's weighting functions. Vardy and Brown (2004) evaluated wall shear stress in unsteady pipe flows building on the previous work by Trikha, but their solutions were faster and valid for both laminar and turbulent flows. Vardy and Hwang (1991) adopted a five-region turbulence model and a different expression in each region to compute the eddy viscosity distribution. Silva-Araya (1993) incorporated an energy dissipation factor to compute laminar and turbulent unsteady friction losses. Brunone et al. (1991) proposed a model where the total friction was the sum of a qusi-steady friction and an unsteady friction that depended on the instantaneous local and convective acceleration. Bergant et al. (2001) incorporated the two unsteady friction models by Zielke (1968) and Brunone et al. (1991) into MOC and compared the results against experiments. They found the Brunone model to be computationally effective. Saikia and Sarma (2006) proposed a numerical model using MOC and unsteady

friction calculated at every time step using Barr's (1980) explicit friction factor correlation.

Water hammer in injectors have been modeled by Moos et al. (2006) and Wang et al. (2008) as a Stoneley wave of amplitude given by Joukowsky's formula (Eq. 1.1) that propagates down the wellbore. Moos et al. (2006) have also demonstrated that using the known physics of Stoneley wave propagation and attenuation in rocks, the formation permeability and porosity can be estimated from water hammer data.

1.1.2 Fracture Impedance

Khalevin (1960), Walker (1962) and Morris et al. (1964) have used acoustic waves to detect wellbore fractures. Mathieu (1984) derived analytically that Stoneley waves could be used to detect hydraulic fractures by realizing that the presence of a fracture changed the acoustic impedance of the wellbore. Mathieu derived the reflection and the transmission coefficients for waves in fractured wellbore and introduced the term "fracture impedance". Hornaby et al. (1989) and Tang and Cheng (1989) subsequently extended Mathieu's work to vertical and horizontal fractures. Medlin (1991) introduced tube waves (very low frequency Stoneley waves) to detect high permeability fractured zones and the connectivity of such zones with the cased hole. Holzhausen et al. (1985, 1986) proposed that the altered acoustic impedance due to a fracture in the wellbore could also be demonstrated and analyzed by the characteristics of pressure oscillations at the wellhead. A single artificially induced pressure pulse at the surface would propagate down the wellbore, get reflected and be transmitted back to the surface. This Hydraulic Impedance Testing (HIT) used a lumped resistance-capacitance in series to model the fracture and estimate the fracture impedance from the reflected pulse by trial and error. The amplitude of the reflected pulse, which is determined by the impedance contrast

between the wellbore and the fracture, could be used to compute the width and height of the fracture. Holzhausen's model was experimentally validated by Paige et al. (1992) and some field scale tests were also carried out (Paige et al., 1993; Holzhausen and Egan, 1986). Paige et al. (1992) showed that the pressure wave would reach the tip of the fracture and proposed that the length of the fracture could be estimated, by measuring the time lapse between the reflections of the wave from the entrance to the fracture and the tip of the fracture. Ashour (1994) generalized Holzhausen's HIT method for vertical and horizontal hydraulic fractures and showed that sending a wave that is close to the resonance frequency of the fracture can make a more accurate assessment of fracture dimensions. Holzhausen's model assumed no energy losses in the wellbore, which meant that the attenuation of the pressure wave due to friction in the wellbore was not taken into consideration. Patzek and De (2000) overcame this issue by proposing a lossy transmission line model to describe the wellbore and fracture geometry and capture the wellbore and fracture dynamics. In their model, flow through both the wellbore and the fracture was treated analogous to the flow of electricity through transmission lines and resistance, capacitance and inductance were distributed over the length of the line. However, it has been the general opinion that it is difficult to collect the required information from the measured pressure signal and HIT has not been used very popularly in the industry.

Chapter 2: Model Formulation

2.1 WATER HAMMER MODELING EQUATIONS

The basic differential equations for transient flow in closed conduits are the one-dimensional conservation equations of mass (continuity equation) and momentum (equation of motion). The generalized forms of these equations were derived by using the Reynolds transport theorem and then simplified using assumptions that are valid for water hammer analysis (Chaudhury, 1987). Wylie and Streeter (1993) have also provided a detailed derivation and discussion of these governing equations. The following sections present a brief description of these equations from their work.

2.1.1 Continuity Equation

The general form of the continuity equation is

$$\frac{1}{\rho}\frac{d\rho}{dt} + \frac{1}{A}\frac{dA}{dt} + \frac{\partial V}{\partial x} = 0 \tag{2.1}$$

where, A = area of cross-section of conduit, ρ = density of the fluid, V = mean flow velocity, t = time, x = coordinate axis along the axis of the conduit. The first term in Eq. (2.1) accounts for the compressibility of the fluid and the second term represents the rate of deformation of the conduit wall.

Assuming an elastic conduit filled with a slightly compressible fluid, Eq. (2.1) simplifies to

$$\frac{\partial p}{\partial t} + V\frac{\partial p}{\partial x} + \rho a^2\frac{\partial V}{\partial x} = 0 \tag{2.2}$$

where, p = pressure intensity, V = mean flow velocity, a = wave speed or the velocity of the water hammer waves. For low-Mach-number unsteady flows, the transport term

$V\,\partial p/\partial x$ is small compared to the other terms and may be dropped to yield the simplified continuity equation

$$\frac{\partial p}{\partial t} + \rho a^2 \frac{\partial V}{\partial x} = 0 \tag{2.3}$$

2.1.2 Equation of Motion

The general form of the momentum equation is

$$\frac{\partial V}{\partial t} + V\frac{\partial V}{\partial x} + \frac{1}{\rho}\frac{\partial p}{\partial x} + g\sin\theta + \frac{fV|V|}{2D} = 0 \tag{2.4}$$

where, f = Darcy-Weisbach friction factor, θ = angle of inclination of the pipe and, D = diameter of the pipe.

Once again, the convective transport term, $V\,\partial V/\partial x$ is neglected for low-Mach-number unsteady flows, reducing Eq. (2.4) to

$$\frac{\partial V}{\partial t} + \frac{1}{\rho}\frac{\partial p}{\partial x} + g\sin\theta + \frac{fV|V|}{2D} = 0 \tag{2.5}$$

It is often convenient to analyze pipeline flows by defining pressure, p, in terms of the piezometric head, H and use the discharge, Q, instead of the flow velocity, V.

$$H = \frac{p}{\rho g} + z$$

$$Q = VA \tag{2.6, 2.7}$$

where, p = pressure, g = acceleration due to gravity, ρ = density of the fluid, z = elevation of the pipe above a specified datum, V = mean flow velocity, and, A = area of cross-section of the pipe.

Eqs. (2.3) and (2.5) expressed in terms of H and Q, become:

$$\frac{\partial H}{\partial t} + \frac{a^2}{gA}\frac{\partial Q}{\partial x} = 0$$

$$\frac{\partial Q}{\partial t} + gA\frac{\partial H}{\partial x} + \frac{fQ|Q|}{2DA} = 0 \qquad (2.8, 2.9)$$

2.1.3 Velocity of Water Hammer Waves

The following general expression for the wave propagation velocity a, was presented by Halliwell (1963)

$$a = \sqrt{\frac{K}{\rho\left[1 + (K/E)\psi\right]}} \qquad (2.10)$$

where, ψ = nondimensional parameter that depends on the elastic properties of the conduit, E = Young's modulus of elasticity of the conduit walls, K = bulk modulus, and ρ = density of the fluid, respectively.

Expressions of ψ under various conditions (rigid conduit, thick-walled elastic conduits, thin-walled elastic conduits, tunnels through solid rock, reinforced concrete pipes, etc.) are available in the literature (Chaudhry, 1987; Wylie and Streeter, 1993). For our analysis, we use the expression of ψ, valid for thin-walled elastic conduits anchored against longitudinal movement throughout its length, given as

$$\psi = \frac{D}{e}\left(1 - \nu^2\right) \qquad (2.11)$$

where, D = conduit diameter, e = wall thickness, ν = Poisson's ratio of pipe material.

2.2 METHOD OF CHARACTERISTICS

The water hammer modeling equations are a pair of quasi-linear, hyperbolic, partial differential equations and a closed-form solution of these equations is not

available. However, there are several methods to numerically integrate these equations, such as, method of characteristics, explicit and implicit finite-difference methods, finite-element methods, etc. Amongst these, the method of characteristics has been the most popular due to its several advantages over other methods, particularly in water hammer type problems. These advantages include an explicit form of solution such that different elements can be solved independently and complex pipe networks can be handled with ease, an established stability criterion, an easy to program and computationally efficient procedure and most importantly, accurate solutions. The main disadvantage of this method is the requirement to adhere to the time step-distance interval relationship.

The momentum and continuity equations, in terms of two dependent variables, discharge and piezometric head, and two independent variables, distance along the pipe and time, are transformed into four ordinary differential equations by the method of characteristics. For further discussion let us rewrite the momentum and continuity equations (Eqs. 2.8 and 2.9) as

$$L_1 = \frac{\partial Q}{\partial t} + gA\frac{\partial H}{\partial x} + \frac{fQ|Q|}{2DA} = 0$$

$$L_2 = a^2\frac{\partial Q}{\partial x} + gA\frac{\partial H}{\partial t} = 0 \qquad (2.12, 2.13)$$

A linear combination of these equations using an unknown multiplier λ yields

$$L = L_1 + \lambda L_2 = \left(\frac{\partial Q}{\partial t} + \lambda a^2\frac{\partial Q}{\partial x}\right) + \lambda gA\left(\frac{\partial H}{\partial x} + \frac{1}{\lambda}\frac{\partial H}{\partial t}\right) + \frac{fQ|Q|}{2DA} = 0 \qquad (2.14)$$

Please note that, using any two real, distinct values of λ, Eq. (2.14) will again yield two equations that are equivalent to Eqs. (2.12) and (2.13). Also, if $H = H(x,t)$ and $Q = Q(x,t)$, then the total derivative can be written as

$$\frac{dH}{dt} = \frac{\partial H}{\partial t} + \frac{\partial H}{\partial x}\frac{dx}{dt}$$

$$\frac{dQ}{dt} = \frac{\partial Q}{\partial t} + \frac{\partial Q}{\partial x}\frac{dx}{dt} \qquad (2.15, 2.16)$$

It can be seen by from Eqs. (2.14), (2.15) and (2.16), that if λ is defined as

$$\frac{1}{\lambda} = \frac{dx}{dt} = \lambda a^2$$

$$\text{i.e.,} \quad \lambda = \pm\frac{1}{a} \qquad (2.17)$$

Then, by substituting the two particular values of λ, Eq. (2.14) can be written as two pairs of equations and identified as C^+ and C^- equations.

$$C^+ : \begin{cases} \dfrac{dQ}{dt} + \dfrac{gA}{a}\dfrac{dH}{dt} + \dfrac{f}{2DA}Q|Q| = 0 \\ \dfrac{dx}{dt} = +a \end{cases}$$

$$C^- : \begin{cases} \dfrac{dQ}{dt} - \dfrac{gA}{a}\dfrac{dH}{dt} + \dfrac{f}{2DA}Q|Q| = 0 \\ \dfrac{dx}{dt} = -a \end{cases} \qquad (2.18, 2.19)$$

Thus, by imposing a relationship between the two independent variables, the original partial differential equations (Eqs. 2.8 and 2.9) were converted to two total differential equations. These ordinary differential equations, however, are not valid everywhere in the *x*-*t* plane like the Eqs. (2.8) and (2.9) were. Instead, Eq. (2.18) and Eq. (2.19) is only valid along straight lines (if *a* is constant) with slope $+1/a$ and $-1/a$ in the

x-t plane, respectively. These lines are called *characteristic lines* and are shown in Fig. 2.1.

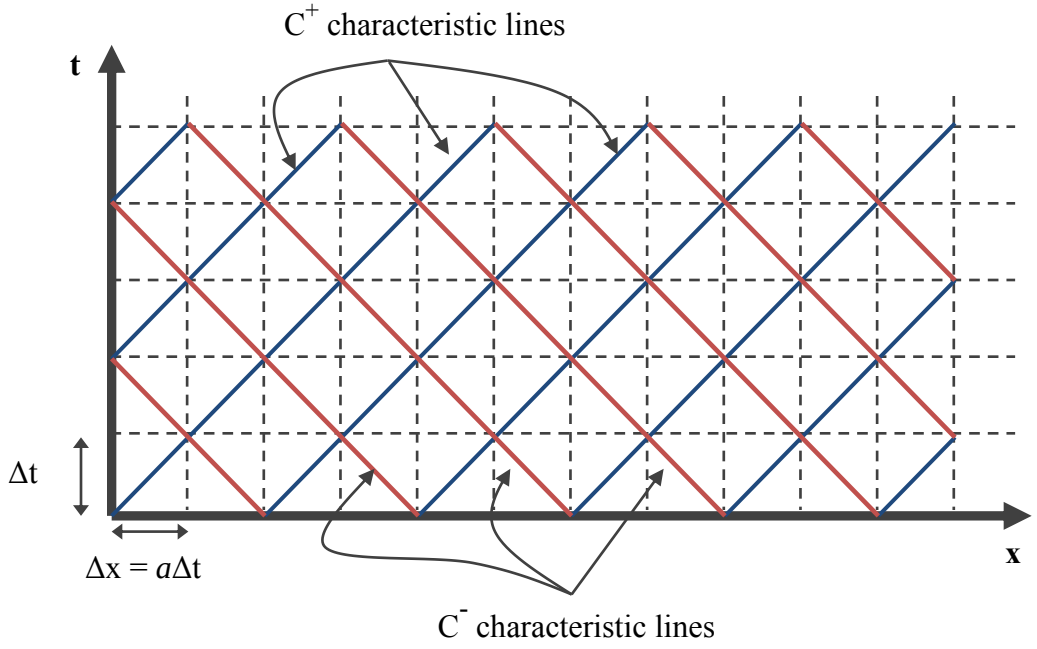

Figure 2.1: Characteristic grid in the *x-t* plane.

Physically, these lines represent the path travelled by a disturbance. For example, a disturbance at point *A* (Fig. 2.2) at time t_0 would travel to point *P* after time Δt .

Thus, we now have two ordinary differential equations and two unknowns, head *H* and discharge *Q*. The unknowns can be calculated at all the points of intersection of the characteristic lines, by integrating the differential equations in finite difference form and solving them simultaneously.

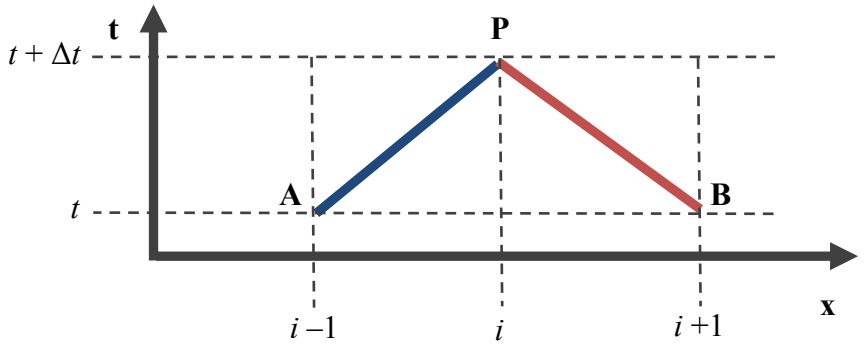

Figure 2.2: Characteristic lines in the *x*-*t* plane.

2.2.1 Finite Difference Equations

A pipeline is divided into an even number of reaches, n, each Δx in length as shown in Fig. 2.1. A time-step is fixed at, $\Delta t = a\,\Delta x$. If the dependent variables, H and Q, are known at A (Fig. 2.2) then Eq. (2.18), which is valid along the positively sloped diagonal (C^+ characteristic line) can be integrated along AP and expressed in terms of the unknown H and Q at P. Similarly, with conditions known at B, Eq. (2.19) valid along the C^- characteristic, can be integrated to yield a second equation in terms of the same unknown H and Q at P.

$$\int_{H_A}^{H_P} dH + \frac{a}{gA}\int_{Q_A}^{Q_P} dQ + \frac{f}{2gDA^2}\int_{x_A}^{x_P} Q|Q|dx = 0 \tag{2.20}$$

The last term in this integration is unknown a priori, and can be written as a first-order approximation as

$$\int_{x_A}^{x_P} Q|Q|dx = Q_A|Q_A|(x_P - x_A) \tag{2.21}$$

or, as a second-order approximation as

$$\int_{x_A}^{x_P} Q|Q|dx = Q_P|Q_A|(x_P - x_A) \tag{2.22}$$

The second-order approximation was used in this analysis, and after integrating as explained, the two difference equations become

$$C^+: \quad H_P = H_A - B(Q_P - Q_A) - RQ_P|Q_A| \tag{2.23}$$

$$C^-: \quad H_P = H_B + B(Q_P - Q_B) + RQ_P|Q_B| \tag{2.24}$$

where, B is the pipeline characteristic impedance:

$$B = \frac{a}{gA} \tag{2.25}$$

and, R is the pipeline resistance coefficient:

$$R = \frac{f\Delta x}{2gDA^2} \tag{2.26}$$

The friction factor f is calculated by the Chen equation (Chen, 1979) at each time step during calculations.

$$\frac{1}{\sqrt{f}} = -2\log\left[\frac{1}{3.7065}\left(\frac{e}{D}\right) - \frac{5.0452}{\mathrm{Re}}\left(\log\left[\frac{1}{2.8257}\left(\frac{e}{D}\right)^{1.1098} + \frac{5.8506}{\mathrm{Re}^{0.8981}}\right]\right)\right] \tag{2.27}$$

where, e = pipe roughness, D = pipe diameter and Re = local Reynolds number calculated at every section at each time step.

The solution to a problem begins at steady-state conditions at time $t = 0$, so H and Q at each section in the pipe is known. The solution proceeds by calculating H and Q at any grid intersection point i at time $t = \Delta t$, from the known conditions at points i-1 and i+1 from the preceding time step, $t = 0$ (as shown in Fig. 2.2). Thus, Eqs. (2.23) and (2.24) may be written as,

$$C^+: \quad H_i^{t+\Delta t} = C_P - B_P Q_i^{t+\Delta t} \tag{2.28}$$

$$C^- : \quad H_i^{t+\Delta t} = C_M + B_M Q_i^{t+\Delta t} \tag{2.29}$$

$$C_P = H_{i-1}^t + BQ_{i-1}^t \tag{2.30}$$

$$B_P = B + R\left|Q_{i-1}^t\right| \tag{2.31}$$

$$C_M = H_{i+1}^t - BQ_{i+1}^t \tag{2.32}$$

$$B_M = B + R\left|Q_{i+1}^t\right| \tag{2.33}$$

where, subscript *i* refers to any grid intersection point, C_P, B_P, C_M and B_M are known constants. Solving them simultaneously,

$$H_i^{t+\Delta t} = \frac{C_P B_M + C_M B_P}{B_P + B_M} \tag{2.34}$$

$$Q_i^{t+\Delta t} = \frac{C_P - C_M}{B_P + B_M} \tag{2.35}$$

However, at the end points of the grid, only one of the characteristics equations is available, hence another relationship between *H* and *Q* must be provided to yield a simultaneous equation. These relationships are called boundary conditions.

2.2.2 Nomenclature

So far, we had been dealing with single pipe systems. Before we go further, it is necessary to explain the nomenclature scheme, used in this analysis, to reference variables (shown in Fig. 2.3). To model a complete well, it is often necessary to describe the well diagram as conduits or pipes with different properties (diameters, wall thickness, etc.) connected in series. The first subscript refers to the conduit number (also referred to

as *section* number). Furthermore, each section or conduit is divided into a number of reaches or subsections for the finite difference calculations. The second subscript refers to the number of the subsection within a particular section. Finally, the superscript, if included, refers to the time step of the calculation.

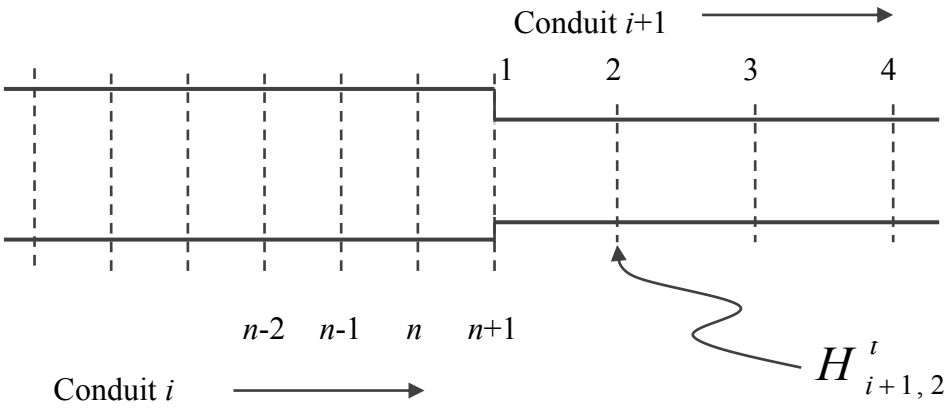

Figure 2.3: Nomenclature scheme for water hammer analysis.

2.3 BOUNDARY CONDITIONS

It can be seen from Fig. 2.1 that at the ends of a pipe, only one of the characteristic equations is available. For the upstream end, the C^- characteristic is available, and for the downstream end, the C^+ characteristic is present. To calculate pressure and discharge at the ends, another relationship is necessary that specifies H_P, Q_P or some relation between them (Fig. 2.2). Any text on water hammer discusses various boundary conditions such as pumps, valves, orifice, etc., and their formulation. For our analysis, we only deal with three boundary conditions that are a) flowrate as a specified function of time at upstream end, b) series connection at the junction of pipes with different properties (diameter, roughness, thickness, etc.) and, c) a porous media/formation at the downstream end.

2.3.1 Flowrate as a Specified Function of Time at Upstream End

The change in flow at the upstream end due to the closing of a valve has been expressed as a function of time. The opening or closing of a valve may be represented by specifying τ versus t (as shown in Fig. 2.4) in a tabular form or as an analytical expression, where τ is the fractional area of the valve open and t is time.

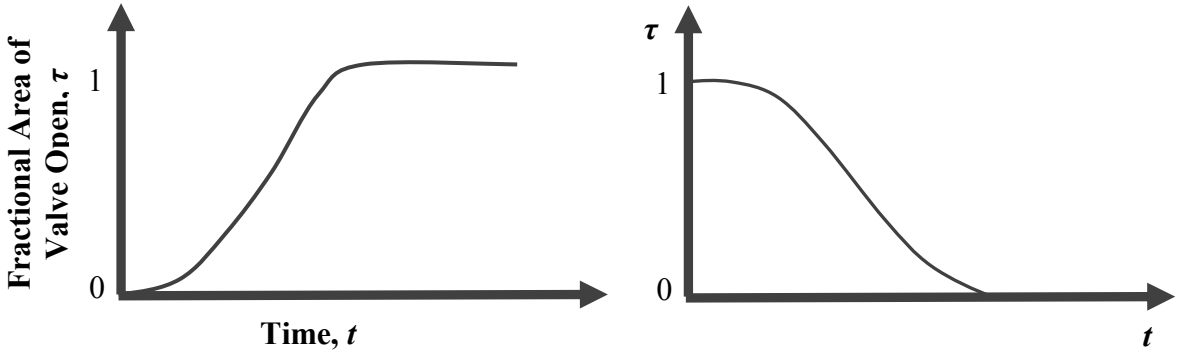

Figure 2.4: Valve opening and closing as a function of time.

The discharge, Q, through the valve is then expressed as,

$$Q_{1,1}^{t} = Q_0 \tau(t) \tag{2.36}$$

where, Q_0 is the steadystate flowrate. The other equation, valid at this point, is Eq. (2.28), and together they may be solved to determine the unknown variables at every time step.

2.3.2 Series Connection

A series connection describes the junction of two conduits having different diameters, wall thicknesses, materials and/or friction factors as shown in Fig. 2.4. If the head losses at the junction are neglected, then it follows that

$$H_{i,n+1} = H_{i+1,1} \tag{2.37}$$

The positive and negative characteristic equations hold for sections i and i+1 respectively and it follows from Eqs. (2.28) through (2.33) as,

$$H_{i,n+1}^{t+\Delta t} = C_{P,i} - B_{P,i}\, Q_{i,n+1}^{t+\Delta t} \tag{2.38}$$

$$C_{P,i} = H_{i,n}^{t} + B_i Q_{i,n}^{t} \tag{2.39}$$

$$B_{P,i} = B_i + R_i \left| Q_{i,n}^{t} \right| \tag{2.40}$$

$$H_{i+1,1}^{t+\Delta t} = C_{M,i+1} + B_{M,i+1}\, Q_{i+1,1}^{t+\Delta t} \tag{2.41}$$

$$C_{M,i+1} = H_{i+1,2}^{t} + B_{i+1} Q_{i+1,2}^{t} \tag{2.42}$$

$$B_{M,i+1} = B_{i+1} + R_{i+1} \left| Q_{i+1,2}^{t} \right| \tag{2.43}$$

Also, from the continuity equation at the junction,

$$Q_{i,n+1} = Q_{i+1,1} \tag{2.44}$$

Therefore, it follows from Eqs. (2.38) through (2.44),

$$Q_{i,n+1}^{t+\Delta t} = Q_{i+1,1}^{t+\Delta t} = \frac{C_{P,i} - C_{M,i+1}}{B_{P,i} + B_{M,i+1}} \tag{2.45}$$

The other unknowns can be calculated directly from the respective equations.

2.3.3 Downstream Boundary Condition

So far, we had developed our model on the lines of traditional water hammer analysis in pipelines. However, the presence of a porous medium at the downstream/upstream end of an injection/production well makes it different from the traditional pipeline water hammer analysis. That is because, in typical pipeline analysis,

the behavior of the boundary elements (such as pumps, surge tanks, orifices, valves etc.) is well defined. On the other hand, the physical properties of the formation are not only heterogeneous but also uncertain. The boundary condition must also describe the transient response of the formation to a high-frequency pressure or rate *wave* at the sand face. Thus, the conventional equations of pressure response used for pressure transient analysis are unsuitable for this analysis, as they assume a step-change to constant rate or pressure. Theoretically, the one-dimensional radial diffusivity equation, Eq. (2.46), can be used but that would require us to assume radial flow (no fracture present), numerically solve a second-order partial differential equation at every time step, estimate reservoir properties and also make assumptions about the near well-bore pressure profile in the reservoir.

$$\frac{\partial^2 P}{\partial r^2} + \frac{1}{r}\frac{\partial P}{\partial r} = \frac{\phi \mu c_t}{k}\frac{\partial P}{\partial t} \tag{2.46}$$

where, ϕ is the formation porosity, μ is the fluid viscosity, c_t is the total compressibility of the system and k is the formation permeability.

In order to overcome these challenges, the formation was defined as an equivalent electrical circuit with lumped resistive (R), capacitance (C) and inertance/inductance (I) elements. A boundary condition can be defined in the form of Eq. (2.47) and the exact formula of the function f depends on the combination (series, or parallel or a combination of both) of R, C and I required to define the boundary.

$$\frac{\Delta H}{Q} = f(R, C, I) \tag{2.47}$$

This definition has three distinct advantages: a) it accounts for the important characteristics of the formation – resistance to flow, compliance of the

formation/fracture, and, compressibility and inertial effects of the fluid, b) it is a dynamic boundary condition and c) it is simple to couple with the wellbore water hammer equations. For given values of R, C and I, pressure and rate transients can be calculated at any point in the well or at the bottomhole. Alternatively, the numerical values of R, C and I can be obtained from the model by history matching measured water hammer pressure data in a well. Therefore, if R, C and I can be related to fracture properties, then there is the exciting opportunity of setting up an inverse problem and using measured water hammer data as a diagnostic tool to estimate fracture properties. The formulation of this boundary condition is discussed in detail in the next section.

2.3.4 Definition of Hydraulic Impedances

Schönfeld (1951) has systematically studied the analogy of hydraulic, mechanical, acoustic and electrical systems and presented the following definitions.

2.3.4.1 Discharge

Discharge (Q) is defined as the volume of fluid transmitted per unit time. The term *flowrate* has been used interchangeably with *discharge* in this text.

2.3.4.2 Potential

The potential (P) is the hydraulic potential, defined as

$$P = \rho g H = \rho g z + p + \tfrac{1}{2}\rho v^2 \tag{2.48}$$

where, H is the total hydraulic head, z is the elevation above some reference level, p is the fluid pressure, ρ is the density and v is the velocity.

2.3.4.3 Resistance

Friction in a conduit causes a loss of potential for a given discharge, and can be expressed as:

$$\Delta P = RQ \tag{2.49}$$

where, $R = 8\mu l / \pi r^4$ for laminar flow in a round tube of radius *r*. The factor *R* is called the *hydraulic resistance.*

For linear flow through a porous medium,

$$\Delta P = \left(\frac{\mu l}{kA}\right) Q = RQ \tag{2.50}$$

Therefore, the flow *Resistance (R)* is the proportionality constant between the discharge (Q) and the potential difference (ΔP) that is required to maintain that discharge.

2.3.4.4 Capacitance

Consider a change in the volume of liquid stored in a system (ΔV) for a change in potential (ΔP). Hence, $\Delta V = C\Delta P$ or

$$Q = C\frac{dP}{dt} \tag{2.51}$$

where, the factor *C* is the *Capacitance* or the storage of the system.

2.3.4.5 Inertance

Consider a variable discharge through a tube. Ignoring friction for the moment, a potential difference (ΔP) will be required to accelerate or decelerate the flow. The pressure drop required to accelerate the fluid is proportional to the *inertance* of the system.

$$\Delta P = I\frac{dQ}{dt} \tag{2.52}$$

where, the factor *I* is the *Inertance* of the system.

2.3.4.6 Wellbore Impedance

The simplified equations of fluid transients in a pipeline were written as Eq. (2.8) and Eq. (2.9). By comparing with the above-mentioned definitions, the resistance, capacitance, and inertance for the wellbore may be written as follows. The impedances are with respect to hydraulic head (H) and per unit length.

$$R_w = \frac{8\mu_w}{\rho\pi r_w^4} \tag{2.53}$$

$$C_w = \frac{\pi g r_w^2}{a_w^2} \tag{2.54}$$

$$I_w = \frac{1}{\pi g r_w^2} \tag{2.55}$$

2.3.5 Analogous Electrical Circuit Representation

In order to draw the analogous electrical circuit representation of the formation/fracture, it is essential to understand the pressure and flowrate behavior during different operations and flow regimes. It is our primary interest to model water hammer observed at the end of pumping in minifracs and after injector shut-ins.

Fig. 2.5 is the conceptual schematic of a wellbore connected to a fracture after a minifrac job. The fracture is filled with the wellbore fluid without any proppant. There is also filter cake deposition on the fracture walls to minimize leakoff and the flow regime inside the fracture is linear. Also, injection at a steady bottomhole pressure implies a growing fracture and in case the fracture stops growing, the bottomhole injection pressure would increase sharply to maintain the injection rate. Therefore, it can be reasonably assumed that during a minifrac, it is the fluid in the fracture and the volume of the fracture that dominates the pressure-flowrate behavior. This can be represented by a

series combination of R, C and I as shown in Fig. 2.6. In this representation, current (~ flowrate) will stop in the circuit as soon as the capacitor (~ fracture compliance) is charged. Current can keep flowing in the circuit, only if the potential difference (~ net pressure) is increased, or, the impedance of the circuit is decreased. Therefore, an increasing capacitance (~ growing fracture) will mean that current (~ frac fluid) can flow in the circuit (~ fracture) at a constant potential difference (~ net pressure). This is analogous to the pressure-flowrate behavior observed during minifracs. Eq. (2.56) is thus the formulation of the bottomhole boundary condition (Eq. 2.47) for minifracs.

$$\rho g \Delta H = RQ + \frac{1}{C}\int Q\,dt + I\frac{dQ}{dt} \tag{2.56}$$

where, ΔH is the potential difference, and Q is the flow rate.

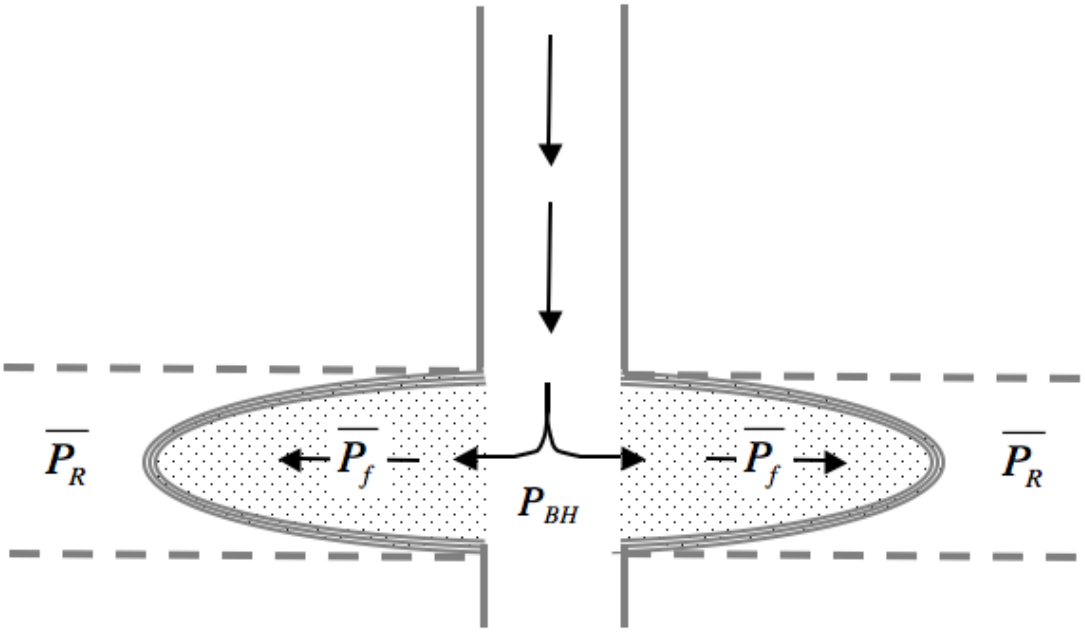

Figure 2.5: Schematic of a minifrac connected to a wellbore.

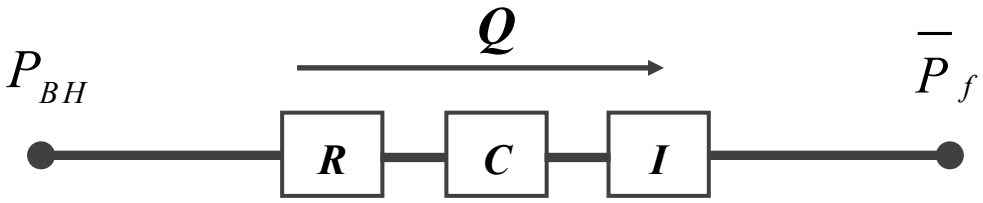

Figure 2.6: Electrical circuit representation of a minifrac.

Schematic of an injection well connected to a formation with a possible fracture is shown in Fig. 2.7. The pressure-flowrate behavior in an injector is different from the minifrac. In injectors, injection rates can be maintained at constant bottomhole pressure for a significantly longer period of time than in minifracs, without the fracture growing as fast. This is because, the fracture is better connected to the formation and the flow regime is possibly pseudo-radial or radial. Also, it can be expected that the fracture, after long periods of injection, is more like a highly conductive porous media than a fluid filled conduit from the minifrac. Thus at steady state, once the compressibility effects have been overcome, the injected fluid flows through the fracture, into the formation and causes the injection front to propagate. The simplest analogous electrical circuit representation of this behavior will be a parallel combination of *R*, *C* and *I* as shown in Fig. 2.8. At steady state, the capacitor is charged and flow is only through the resistance of the circuit for a constant current and potential difference. Eq. (2.57) is the formulation of the bottomhole boundary condition (Eq. 2.47) for injectors. Please note that *R*, *C* and *I*, for injectors are a combination of fracture and/or formation *R*, *C* and *I*, and therefore, an equivalent *R*, *C* and *I*.

$$Q = \rho g\left(\frac{\Delta H}{R} + C\frac{d(\Delta H)}{dt} + \frac{1}{I}\int(\Delta H)dt\right) \tag{2.57}$$

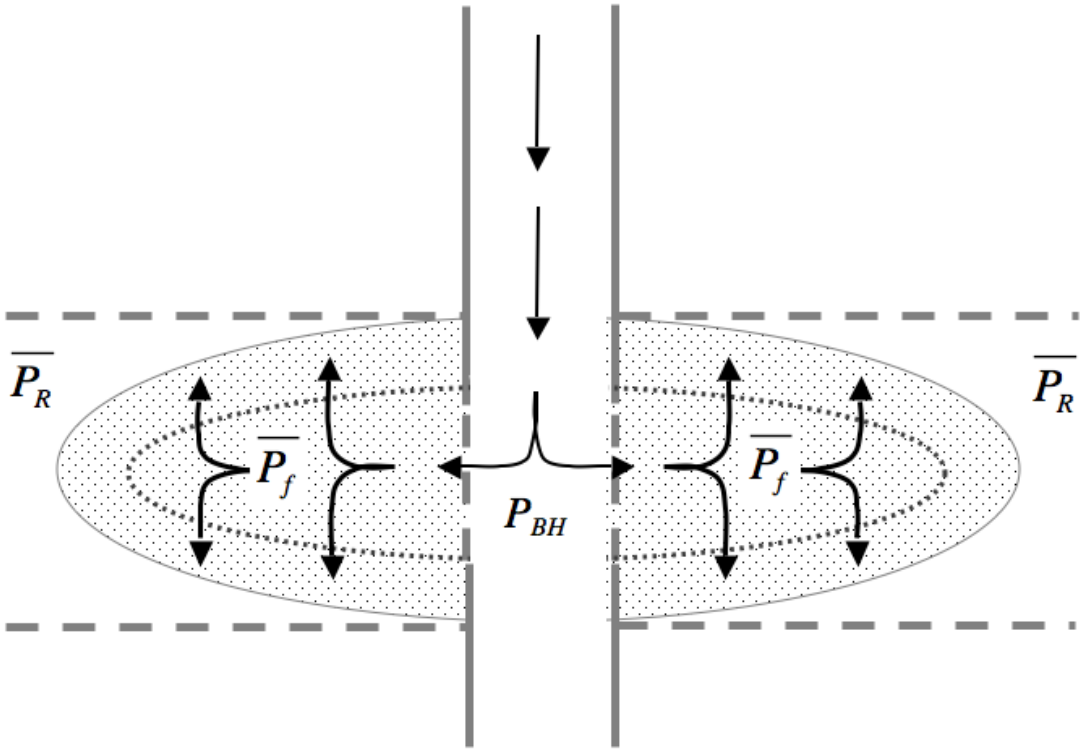

Figure 2.7: Schematic of an injection well.

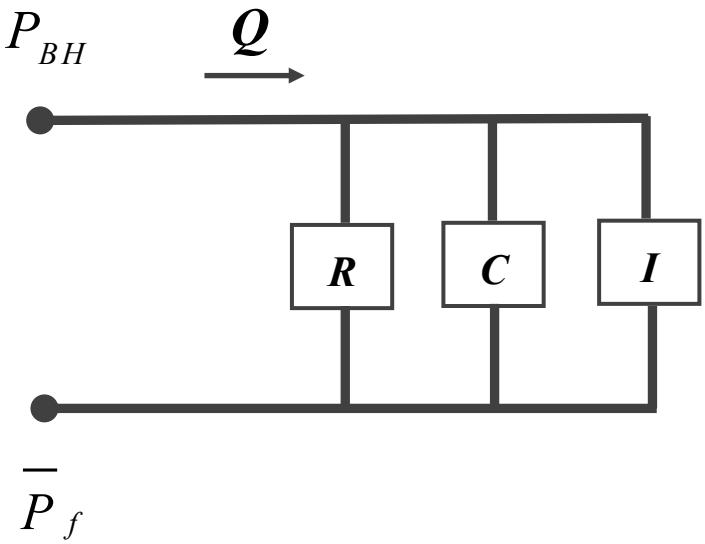

Figure 2.8: Electrical circuit representation of an injector.

The potential difference, ΔH, is defined in Eq. (2.47) as the difference between the bottomhole pressure (P_{BH}) and the average near wellbore pressure ($\overline{P}_f$) at any time. Traditionally, the ISIP is considered to be the average near wellbore pressure because it is assumed that the fluid comes to rest at shut-in and the near wellbore frictional pressure drop, (P_{BH} - ISIP), becomes zero. But, the fluid in the wellbore does not come to rest instantaneously (as proved by a water hammer). Hence, the traditional estimate of ISIP is not completely devoid of the frictional pressure drop and thus not an accurate estimate of the average near wellbore pressure. Therefore, average near wellbore pressure ($\overline{P}_f$) is taken to be different from ISIP.

Water hammer is a fast transient as compared to the pressure transient response of the reservoir. It is a reasonable assumption that the water hammer will not see the far-field reservoir pressure. Hence, the potential difference has been defined with respect to the average near wellbore pressure and not the average reservoir pressure. $\overline{P}_f$ is calculated by fitting an exponential decay curve to the decline part of the measured surface pressure data, where k is the exponential decay constant and P_{f0} is the average near wellbore pressure prior to shut-in.

$$\begin{aligned} \rho g \Delta H &= P_{BH} - \overline{P}_f \\ &= \rho g H_{N,n+1}^{t+\Delta t} - P_{f0} e^{-kt} \end{aligned} \tag{2.58}$$

A conceptual schematic of this is shown in Fig. 2.9. The value of P_{f0} is always between the instantaneous shut-in pressure (ISIP) and the end of water hammer pressure (P_{EoWH}). If the pressure decline rate is low, then P_{EoWH} has been found to be a good estimate of P_{f0}.

This completes the modeling of water hammer in the wellbore. In summary, the inputs that must be provided are the injection fluid properties, the steady state injection

pressure and flowrate, the wellbore geometry specified as a series connection of different pipes and the valve closing characteristics. The bottomhole boundary condition parameters (R, C and I) can be either specified or obtained by history matching the measured data (injection or minifrac water hammer). The model can then be used to estimate bottomhole water hammer pressures.

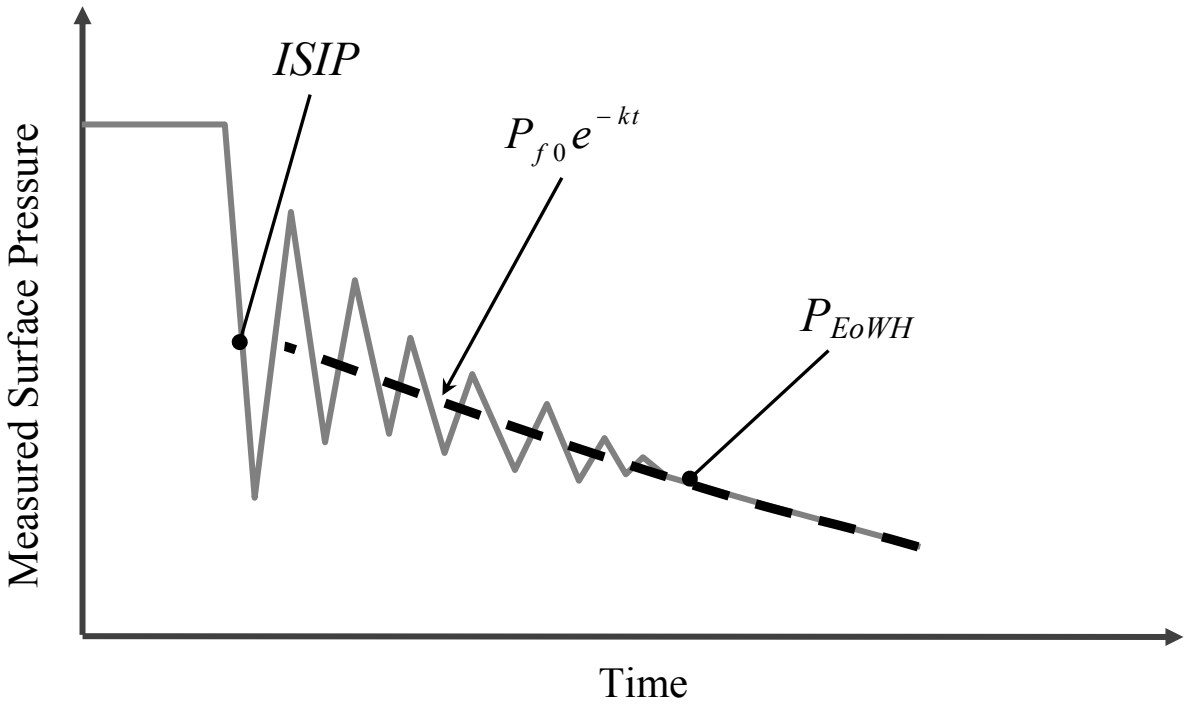

Figure 2.9: Schematic of water hammer decline and near wellbore average pressure.

2.4 FRACTURE IMPEDANCE

2.4.1 Fracture Dimensions from Model Parameters

Once the values of the model parameters (R, C and I) have been estimated by history matching the measured water hammer data, they can be used to calculate fracture dimensions and net fracture overpressures by making the following assumptions:

i. The wellbore interacts with the formation only through the fracture.

ii. A single planar of constant height and ellipsoidal cross-section.

iii. Fracture dimensions do not change during the period of water hammer.

iv. Leakoff through the fracture is negligible during water hammer event.

v. Flow resistance is primarily at the entrance to the fracture and is negligible along its length.

Based on these assumptions, the resistance *R* is due to the near wellbore frictional pressure drop (ΔP_{nwf}) and signifies the connectivity of the fracture with the wellbore.

$$R = \frac{\Delta P_{nwf}}{Q_0} \tag{2.59}$$

where, Q_0 is the injection rate prior to shut-in.

The net pressure is given by the difference between the average pressure inside the fracture $(P_{BH} - \Delta P_{nwf})$ and the minimum horizontal in-situ stress $(S_{h\min})$.

$$\overline{\Delta P_o} = (P_{BH} - \Delta P_{nwf}) - S_{h\min} \tag{2.60}$$

Based on various parameters, the fracture length ($2L_f$) can be either smaller or larger than the fracture height (h_f). In the following text, fractures have been classified as short ($2L_f/h_f < 1$) and long ($2L_f/h_f \geq 1$), and different formulation of capacitance (*C*) and inertance (*I*) have been derived for them based on the work of Shylapobersky et al. (1988). The upper quantities in the bracket are for short fractures and the lower quantities are for long fractures.

$$m = \begin{pmatrix} 1 - \left(2L_f/h_f\right)^2 \geq 0 \\ 1 - \left(h_f/2L_f\right)^2 \geq 0 \end{pmatrix} \tag{2.61}$$

The net pressure can be related to the fracture dimensions as:

$$\overline{\Delta P_o} = \frac{4}{\pi^2}\frac{E}{1-\nu^2}E(m)\bar{w}\begin{pmatrix} 1/L_f \\ 2/h_f \end{pmatrix} \tag{2.62}$$

where, E is the Young's modulus, v is the Poisson's ratio, $\bar{w}$ is the average fracture width, and, $E(m)$ is the complete elliptical integral of the second kind, respectively. The plane strain elastic modulus (E') is defined as:

$$E' = \frac{E}{1-\nu^2} \tag{2.63}$$

Assuming that the change in fracture compliance is only due to a change in width, the capacitance, which was previously defined as $\Delta V/\Delta P$, can be rewritten as:

$$C = \frac{\Delta w h_f L_f}{\Delta P} \tag{2.64}$$

From Eq. (2.62) through (2.64)

$$C = \frac{\pi^2 h_f L_f}{4E'E(m)}\begin{pmatrix} L_f \\ h_f/2 \end{pmatrix} \tag{2.65}$$

Inertance can be defined analogous to the inertance of the wellbore given by Eq. (2.55) and is given as

$$I = \frac{\rho L_f}{\bar{w}h_f} = \frac{4\rho E'E(m)L_f}{\overline{\Delta P_o} h_f}\begin{pmatrix} 1/L_f \\ 2/h_f \end{pmatrix} \tag{2.66}$$

Therefore, using Eqs. (2.59) through (2.66), assuming bottomhole pressure prior to shut-in and minimum in-situ horizontal stress are known, the near wellbore pressure drop and fracture half-length can be calculated as:

$$\Delta P_{nwf} = RQ_0 \tag{2.67}$$

$$L_f = \sqrt{\frac{CI\overline{\Delta P_o}}{\rho}} \tag{2.68}$$

Since, $E(m)$ and $\overline{w}$ are functions of fracture height, h_f and $\overline{w}$ are calculated iteratively by such that Eqs. (2.69) and (2.70) are satisfied.

$$h_f = \begin{cases} \dfrac{4E'E(m)C}{\pi^2 L_f^2} & if\ \left(2L_f / h_f\right) < 1 \\ \sqrt{\dfrac{8E'E(m)C}{\pi^2 L_f}} & if\ \left(2L_f / h_f\right) \geq 1 \end{cases} \tag{2.69}$$

$$h_f = \frac{\rho L_f}{\overline{w} I} \tag{2.70}$$

2.4.2 Estimate of Model Parameters

An initial estimate of R, C and I can be made from estimates/assumptions of fracture height and near wellbore frictional pressure drop. The fracture height may be assumed to be the height of the perforated interval. The near wellbore frictional pressure drop, ΔP_{nwf}, may be calculated as:

$$\Delta P_{nwf} = P_{BH}^{t=0} - P_{f0} \tag{2.71}$$

R can be estimated according to Eq. (2.60). To calculate C and I, estimates of $\overline{w}$ and L_f must first be obtained.

Shylapobersky et al. (1988) formulated an expression for average width by taking into consideration the width due to both viscous dissipation (w_f) and rock toughness

(w_c) effects. In order to distinguish it from the average width definition used previously ($\bar{w}$), this definition of average width will be referred to as w' and is given by:

$$w' = \sqrt{w_c^2 + \sqrt{w_c^4 + w_f^4}} \tag{2.72}$$

where,

$$w_c^2 = \frac{\pi^2 \Gamma}{4E'E(m)} \begin{pmatrix} L_f / G_s(m) \\ h_f / (2G_l(m)) \end{pmatrix} \tag{2.73}$$

$$w_f^4 = \frac{3\pi^4 \mu Q_0 L_f}{8E'E(m)} \begin{pmatrix} L_f / h_f \\ 1/2 \end{pmatrix} \tag{2.74}$$

The geometrical function for short fracture and long fracture is given by:

$$\begin{pmatrix} G_s(m) \\ G_l(m) \end{pmatrix} = \begin{pmatrix} 1.0 - (2L_f / h_f)^2 [K(m) - E(m)] / [2mE(m)] \\ 0.5 + (h_f / 2L_f)^2 [K(m) - E(m)] / [2mE(m)] \end{pmatrix} \tag{2.75}$$

where, $K(m)$ and $E(m)$ are the complete elliptical integral of the first and second kind, respectively (Appendix).

The apparent fracture toughness (Γ) is given for short and long fractures as:

$$\begin{pmatrix} \Gamma_s \\ \Gamma_l \end{pmatrix} = \begin{pmatrix} \dfrac{2(\overline{\Delta P_o})^2 L_f}{\pi E'} \\ \dfrac{\pi^2 (\overline{\Delta P_o})^2 h_f G_l(m)}{32E'E(m)} \end{pmatrix} \tag{2.76}$$

The fracture length is calculated iteratively by equating the two average widths given by Eq. (3.62) and (3.72) respectively. The average fracture width can then be

calculated either definition. Initial estimates of R, C and I can be obtained to run the water hammer model. These estimates can be improved by iteratively matching the measured water hammer data.

Chapter 3: Results and Discussion

3.1 Hydraulic Impedance Testing

To validate our modeling approach, this model was used to simulate a hydraulic impedance test. Instead of a shut-in at the surface (a step change in flowrate), a short duration pressure pulse was generated by momentarily changing the flowrate at the surface. Figs. 3.1 and 3.2 show the results for an open fracture (low resistance, high capacitance) and a closed fracture (high resistance, low capacitance) respectively. The results show that for an open fracture the pressure wave is reflected with an opposite polarity while for a closed fracture the reflected wave has the same polarity as that of the incident wave. This is a well-known observation (Holzhausen et al., 1985; Patzek and De, 2000) and forms the basis of using pressure pulse testing to determine fracture closure pressures. In this case, it confirms that our modeling approach (which is traditional fluid transient analysis by solving conservation of mass and momentum equations but with an impedance boundary condition) can adequately capture the wellbore-fracture dynamics.

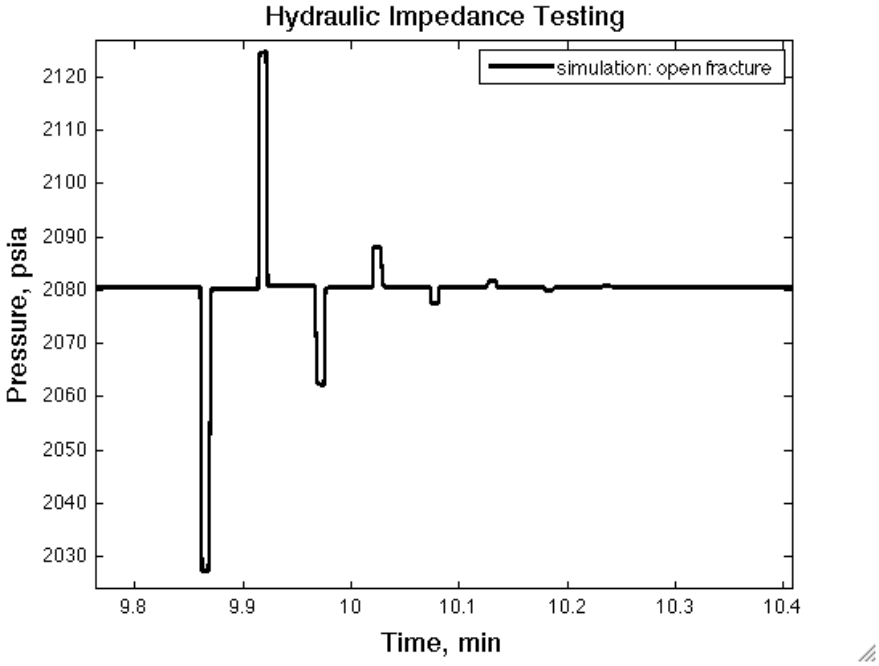

Figure 3.1: Simulated HIT for well with open fracture.

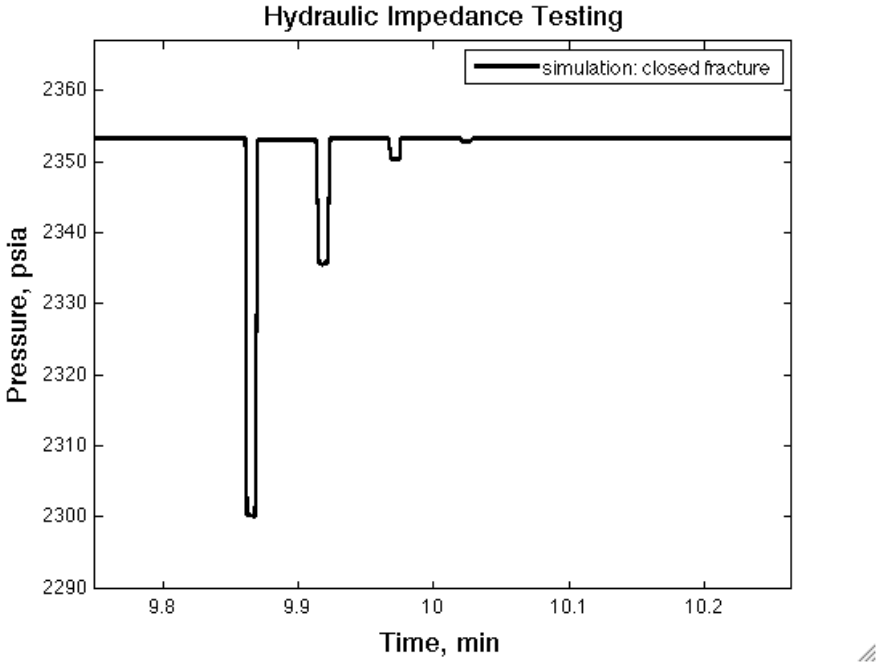

Figure 3.2: Simulated HIT for well with closed fracture.

3.2 History Matching Surface Water Hammer in Injectors

The model was used to simulate several injector water hammer incidents from different fields. In this text we will discuss five injector water hammer cases that were presented by McCarty and Norman (2006). Figs. 3.3 through 3.12 show two plots for each well A through E, respectively. The first figure for each case shows the overall match (amplitude, decay and duration) of the water hammer incident, while the second offers a closer look at the water hammer data and highlights the detailed waveform comparison.

It can be seen that the model shows a good agreement with the measured data for a wide variety of water hammer situations. Wells A, B, and E, in particular, show remarkable agreement between the model and the data. Though the model predicts the overall trend for wells C and D, a closer look at the data reveals that some waveforms are truncated and some apparent wave cycles have been missed in the measurements. This can be attributed to the sensitivity and sampling time of the pressure gauge used to collect the data. As illustrated by Wang et al. (2008) (Fig. 3.13), under-sampling can distort the data and give the impression of longer wave periods or lower frequency of oscillations than might be the actual case. Also, under-sampling can miss some of the pressure peaks showing lower amplitudes. We see evidence of both from the comparison of the modeled water hammer to the measured data. Therefore, it is recommended to use faster gauges to capture the full details of a water hammer. Ideally, a pressure gauge that can at least sample at twice the frequency of the water hammer wave should be used.

3.3 Simulated Bottomhole Water Hammer in Injectors

Figs. 3.14 through 3.18, show the simulated bottomhole water hammer for these cases. It can be observed that in all these cases, the bottomhole water hammer magnitudes are lower than the surface values. The sand face water hammer is in tens of psi whereas

the surface water hammer is in hundreds of psi. The attenuation can be attributed to the friction in the wellbore and damping due to the porous medium.

A conductive formation will cause the water hammer energy to dissipate faster as seen in well E. The well E has the largest near wellbore frictional pressure drop ($P_{inj} - ISIP \sim 600$ psi), which can be identified from the surface pressure data. Though the near wellbore pressure drop is high, the pressure decline is much faster compared to the other wells, which indicates a very conductive formation. The conductive formation in E causes the bottomhole water hammer (Fig. 3.18) to dissipate fast despite a high near wellbore friction.

McCarty and Norman (2006) have stated that wells D and E are excellent injectors. The value of inertance (proportional to the mass in the system) obtained from the model for these two wells are higher than the others, which is in agreement with this observation. Table 3.1 summarizes the values of the model parameters obtained by history matching, the simulated and/or measured surface and bottomhole pressure flux and the estimated degree of attenuation in these cases.

It is shown that under most conditions, due to the attenuated water hammer at the sand face, the primary concern associated with water hammer effects are not wellbore stability. This implies that cross-flow and re-entrainment of fines and filter cakes at the wellbore wall might be leading to significant declines in well injectivity.

The question, whether downhole valve closures are a better alternative to mitigate the water hammer effects, has also been investigated. Fig. 3.19 shows the bottomhole water hammer in well A (Fig. 3.3) for a hypothetical downhole shut-in at a distance of 2000 ft above the sand face. Injection rates and other model parameters have been kept constant. It can be seen that though the magnitude of the water hammer has reduced the frequency of the wave has increased due to a reduced wellbore length. The decrease in

magnitude is due to the increased damping of the pressure wave by the formation as the higher frequency wave interacts more with the formation. However, since the sand face water hammer is still in the same order of magnitude, we believe that the higher frequency of pressure oscillations at the sand face pose greater threat to fines mobilization and the stability of sand bridges. In any case, the reduction is water hammer due to downhole shut-in is only if the formation is favorable and damps out the wave. Fig. 3.20 illustrates a scenario, where there is a downhole shut-in but the bottomhole resistance is higher than the case shown in Fig. 3.19. It can be seen that there is no advantage from the reduction in magnitude but the disadvantage of a higher frequency pressure wave is still present. It is therefore, our recommendation that downhole shut-ins should be avoided.

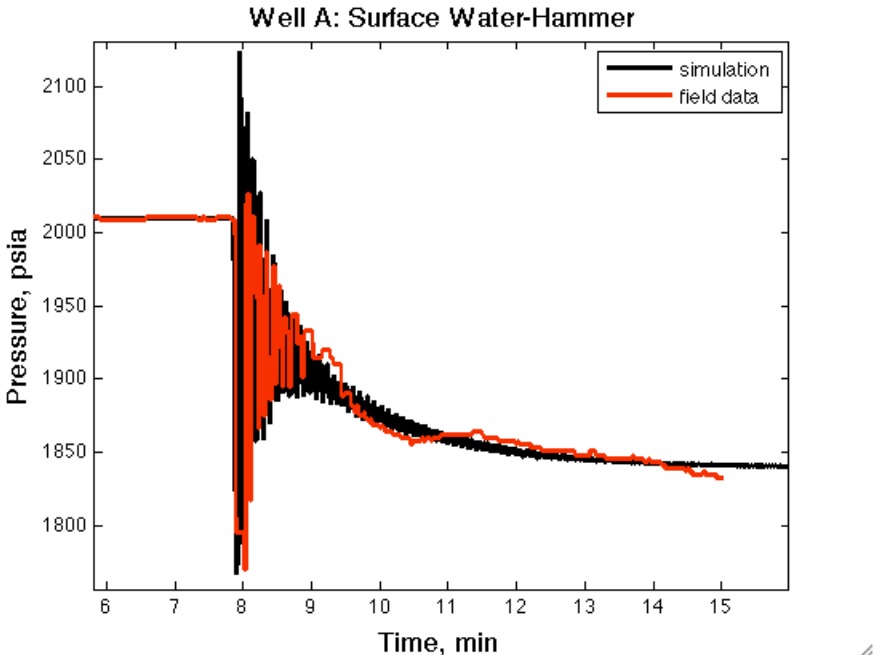

Figure 3.3: History matching overall surface water hammer in Well A.

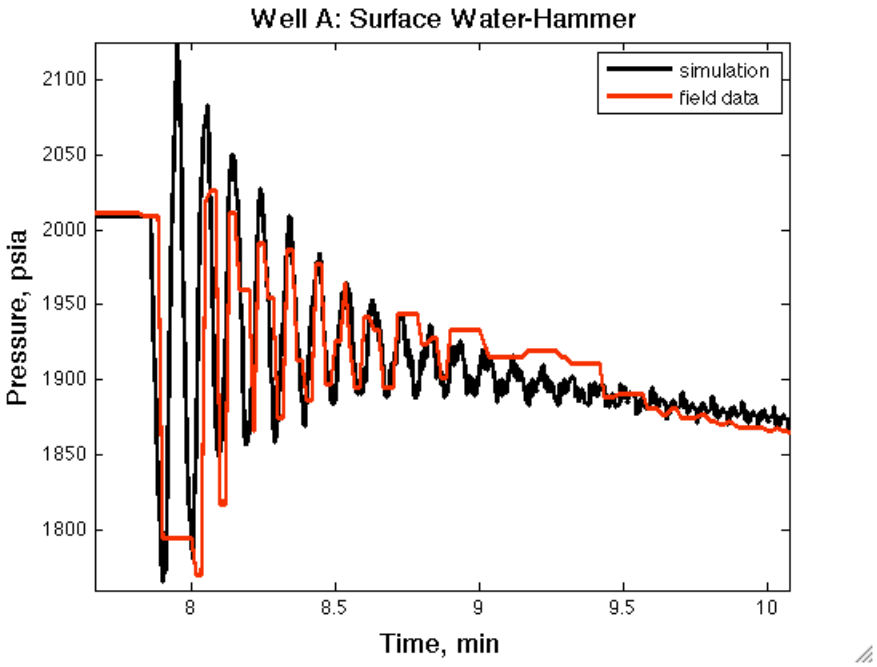

Figure 3.4: Detailed waveform comparison of water hammer in Well A.

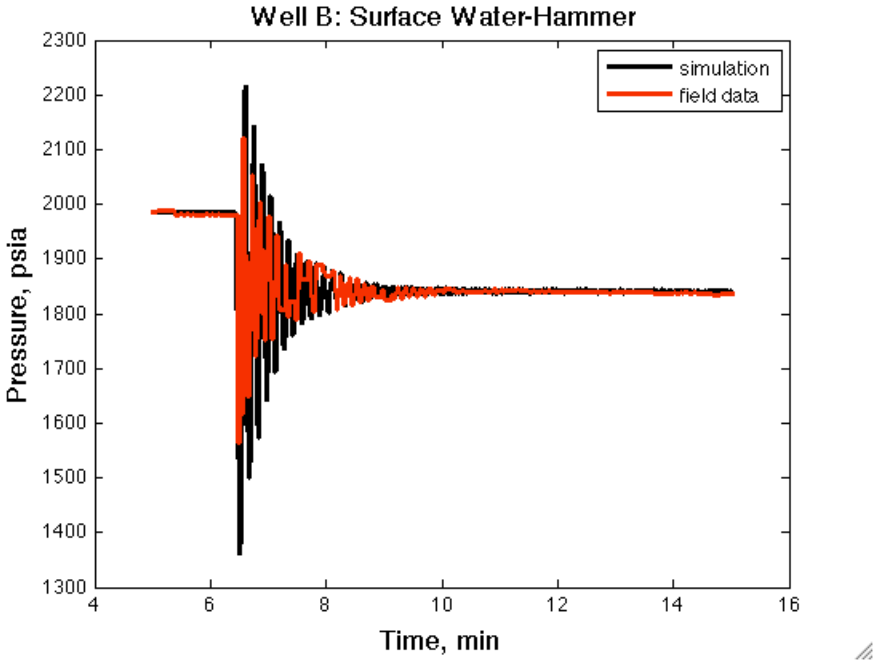

Figure 3.5: History matching overall surface water hammer in Well B.

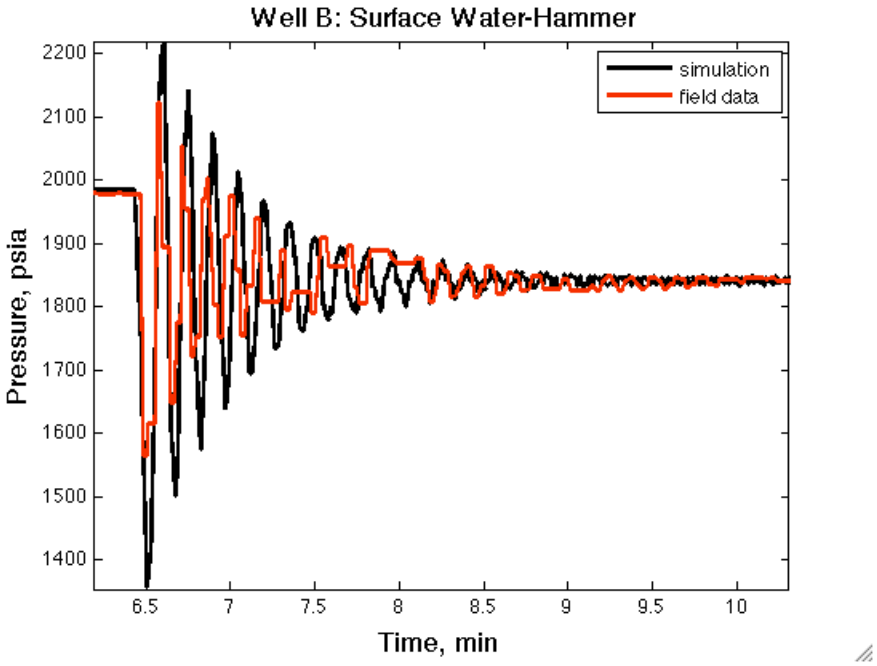

Figure 3.6: Detailed waveform comparison of water hammer in Well B.

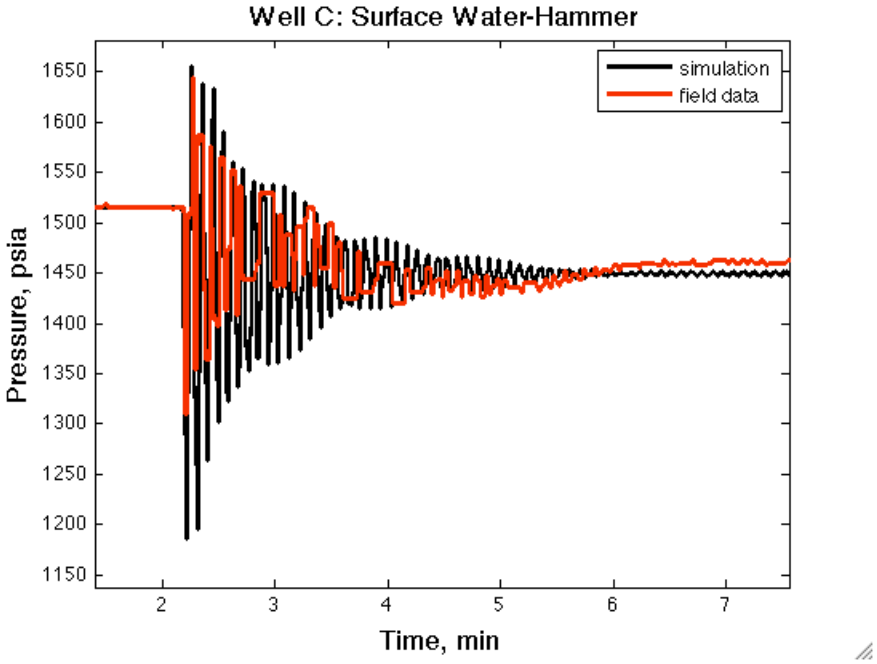

Figure 3.7: History matching overall surface water hammer in Well C.

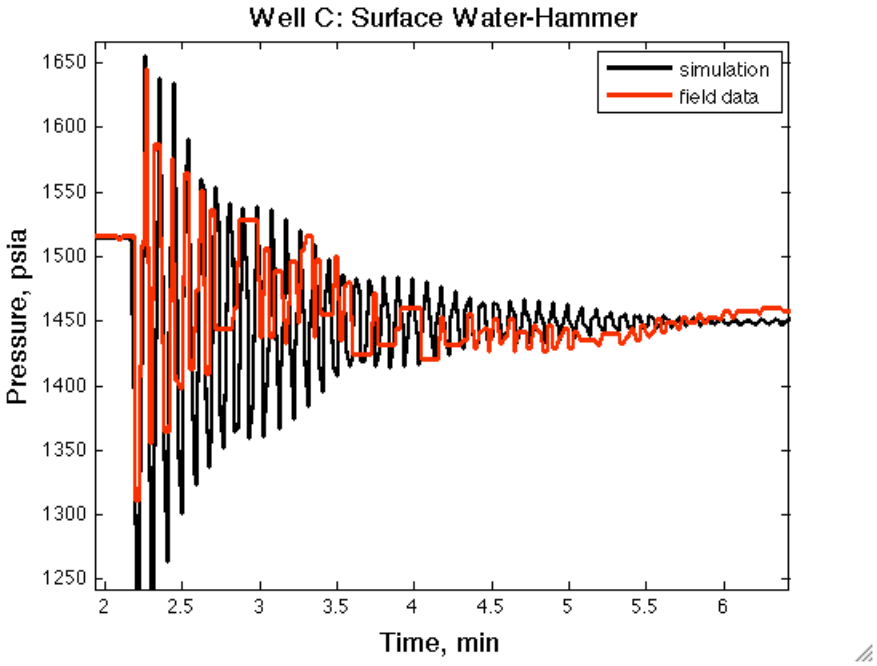

Figure 3.8: Detailed waveform comparison of water hammer in Well C.

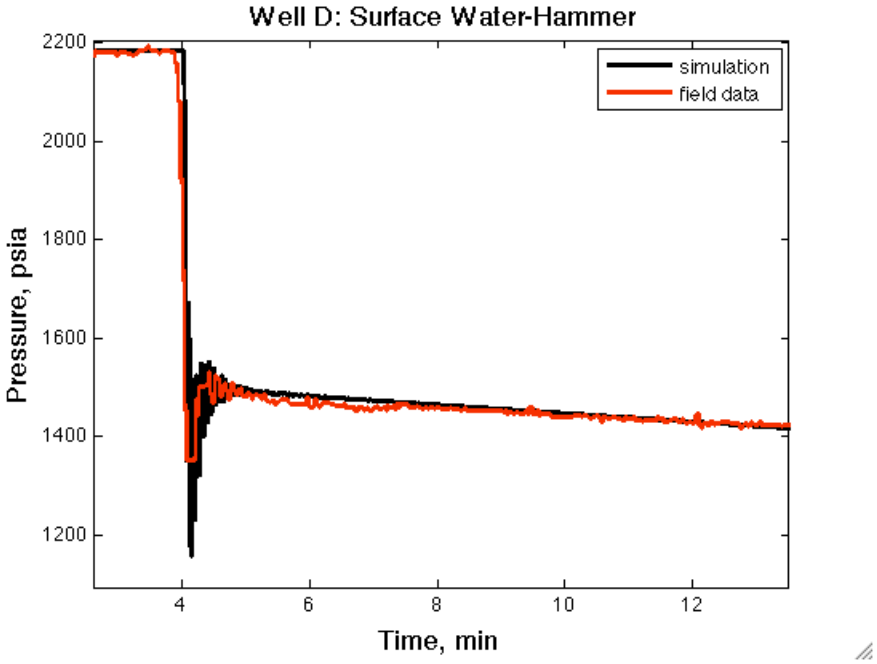

Figure 3.9: History matching overall surface water hammer in Well D.

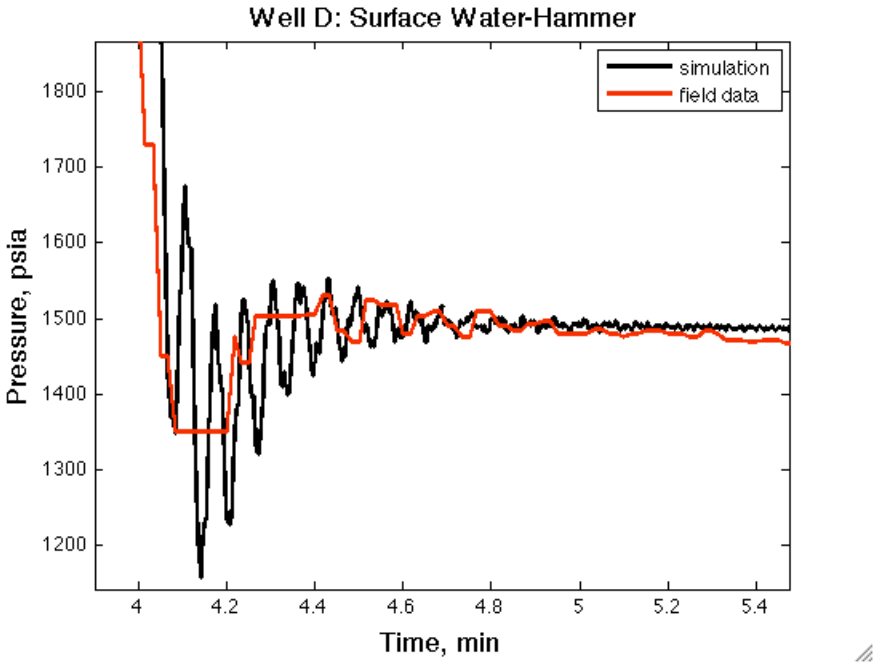

Figure 3.10: Detailed waveform comparison of water hammer in Well D.

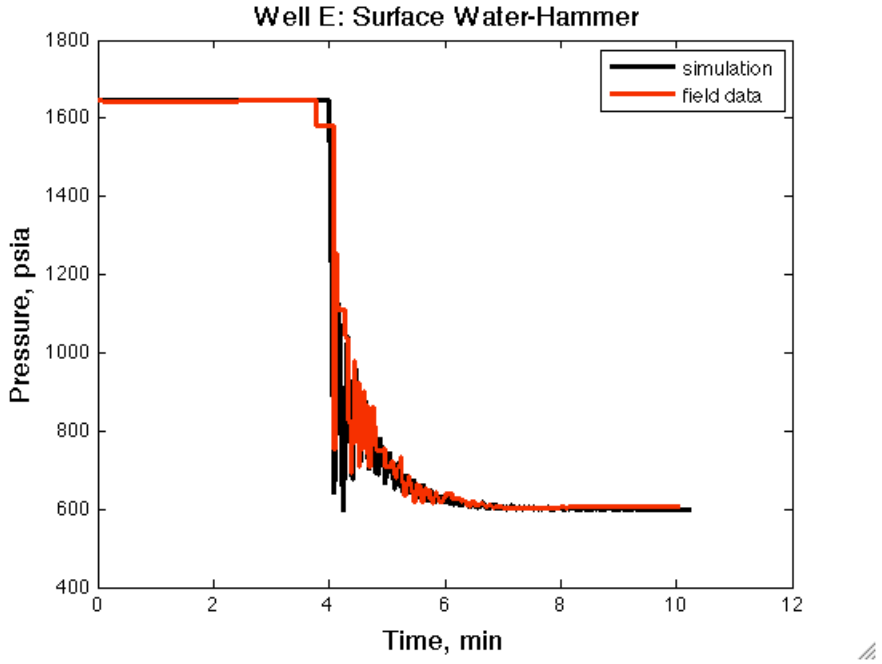

Figure 3.11: History matching overall surface water hammer in Well E.

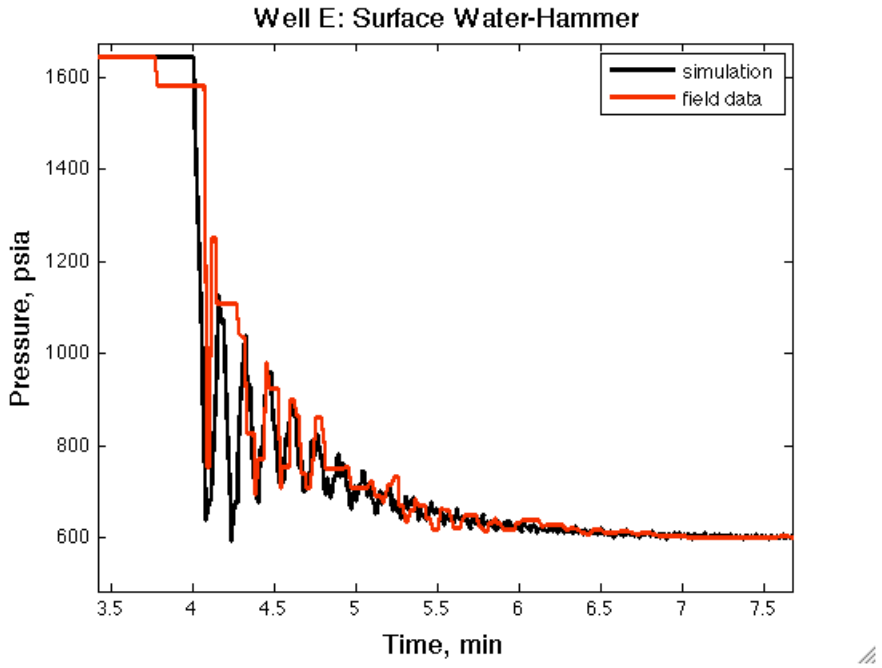

Figure 3.12: Detailed waveform comparison of water hammer in Well E.

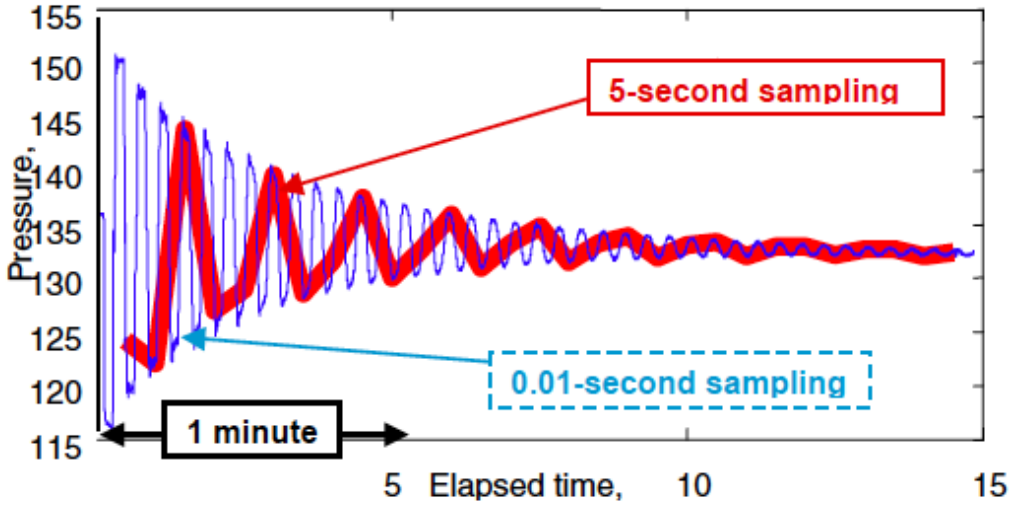

Figure 3.13: Misrepresentation of water hammer data due to the effect of under-sampling (after Wang et al., 2008).

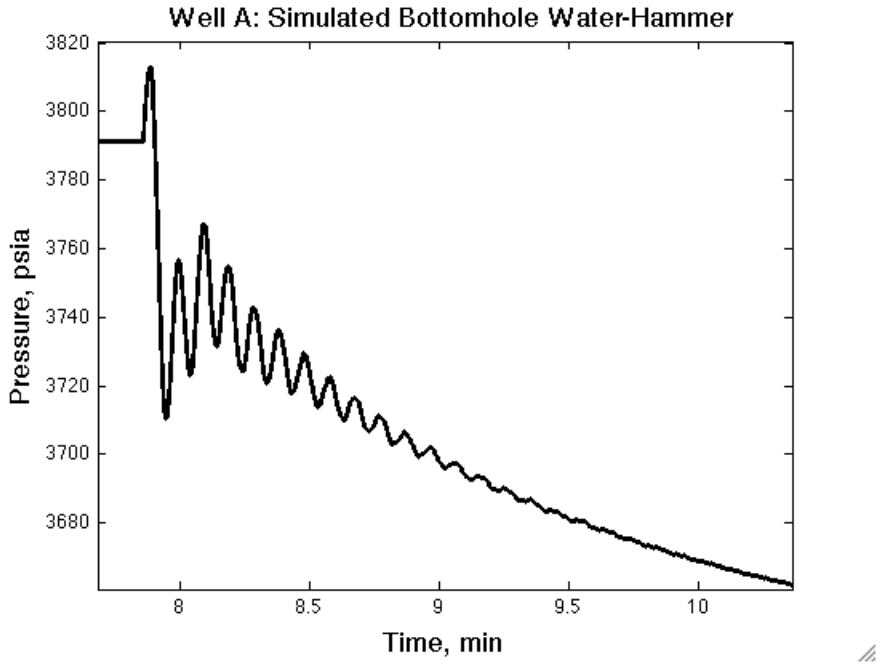

Figure 3.14: Simulated bottomhole water hammer for well A

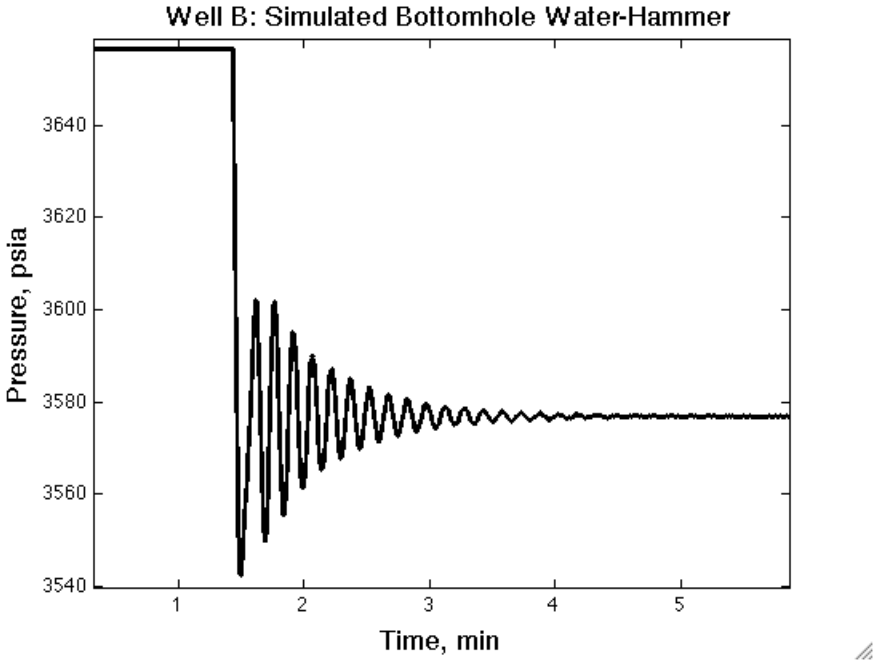

Figure 3.15: Simulated bottomhole water hammer for well B.

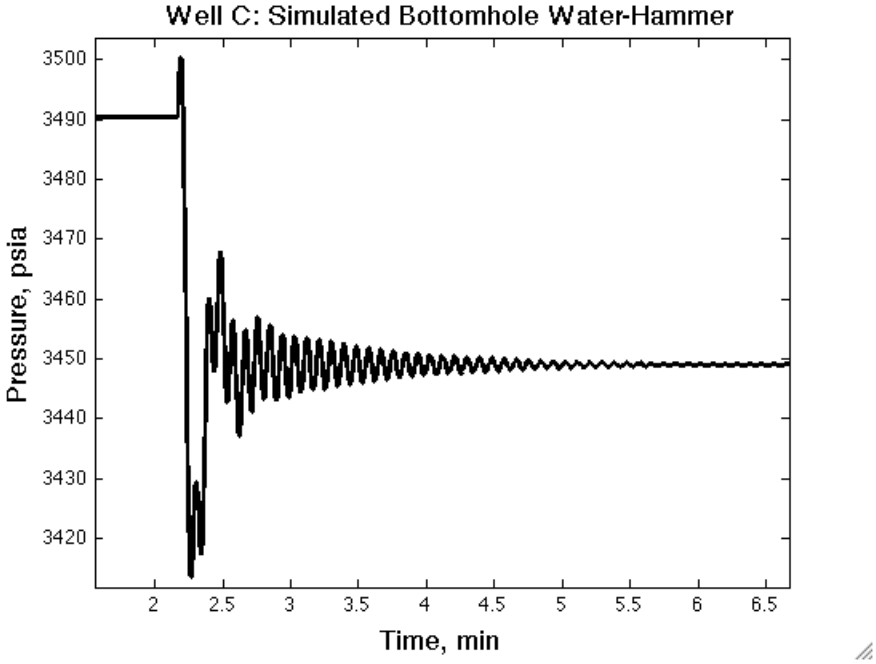

Figure 3.16: Simulated bottomhole water hammer for well C.

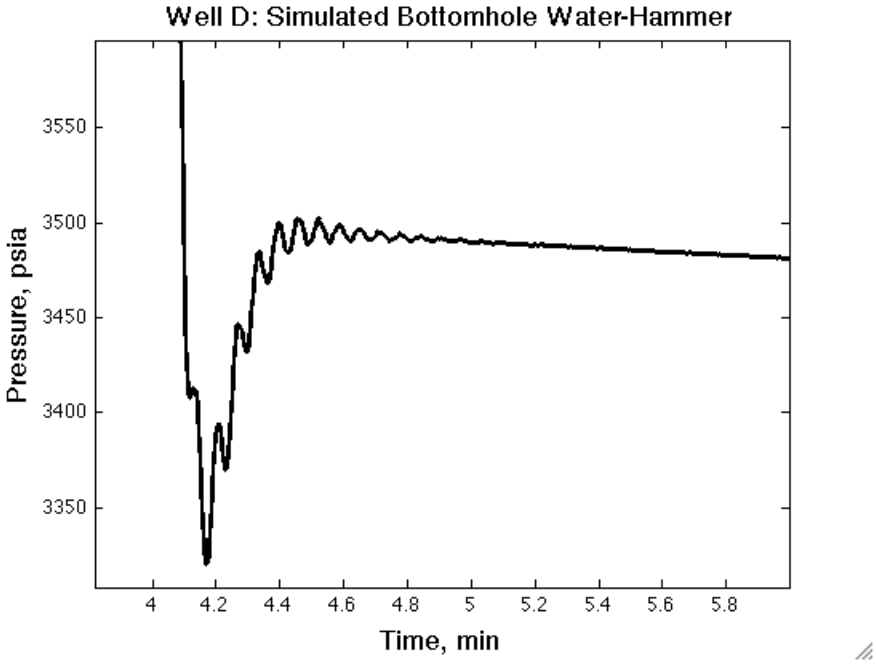

Figure 3.17: Simulated bottomhole water hammer for well D.

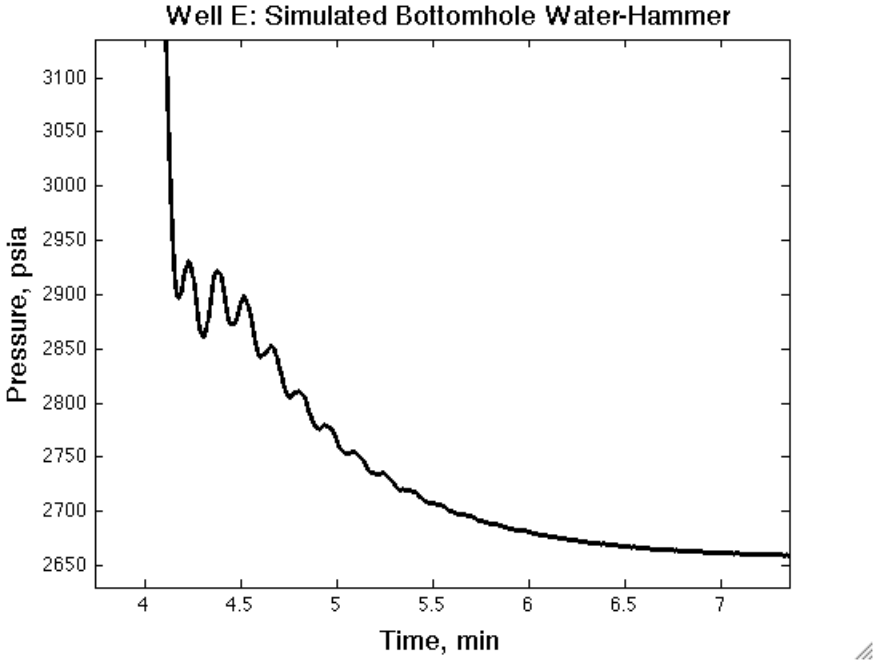

Figure 3.18: Simulated bottomhole water hammer for well E.

Wells	Resistance (bpd/psi)	Capacitance (bbl/psi)	Inertance (psi/bbl/d^2)	$\Delta P_{Surface}$ (psi) (Simulation/Measured)	ΔP_{BH} (psi) (Simulation)	Attenuation $\Delta P_{BH} / \Delta P_{surface}$
A	89.87	2.44×10^{-3}	3.09×10^{-7}	350/265	50	0.14
B	333.9	6.72×10^{-3}	2.45×10^{-8}	850/660	60	0.07
C	74.75	3.29×10^{-3}	3.09×10^{-7}	470/350	60	0.13
D	59.38	1.09×10^{-3}	1.23×10^{-6}	300/180	60	0.20
E	94.11	2.74×10^{-3}	9.77×10^{-7}	500/500	70	0.14

Table 3.1: Summary of model parameters, total surface and bottomhole pressure fluxes and attenuation.

Wells	Resistance (bpd/psi)	Capacitance (bbl/psi)	Inertance (psi/bbl/d^2)	Height (ft)	Half Length (ft)	Width (in)	ΔP_{nwf} (psi)
A	89.87	2.44×10^{-3}	3.09×10^{-7}	4.3	403.3	0.05	94.5
B	333.9	6.72×10^{-3}	2.45×10^{-8}	10.2	198.2	0.12	52.4
C	74.75	3.29×10^{-3}	3.09×10^{-7}	4.7	468.9	0.05	93.6
D	59.38	1.09×10^{-3}	1.23×10^{-6}	3.5	283.5	0.01	387.3
E	94.11	2.74×10^{-3}	9.77×10^{-7}	4.1	507.8	0.02	318.8

Table 3.2: Summary of model parameters, equivalent fracture dimensions and near wellbore frictional pressure drop.

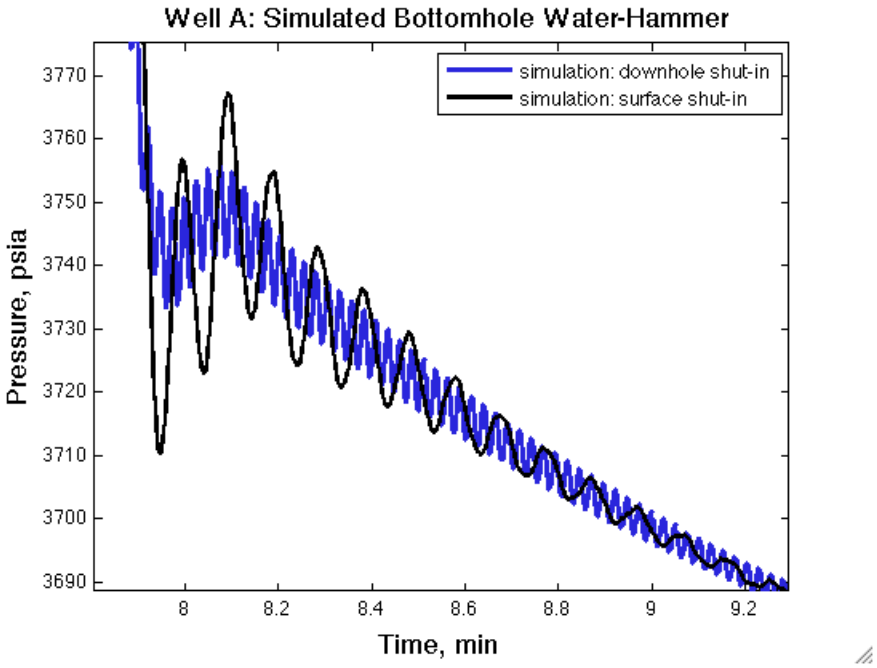

Figure 3.19: Simulated bottomhole water hammer for a downhole shut-in in well A.

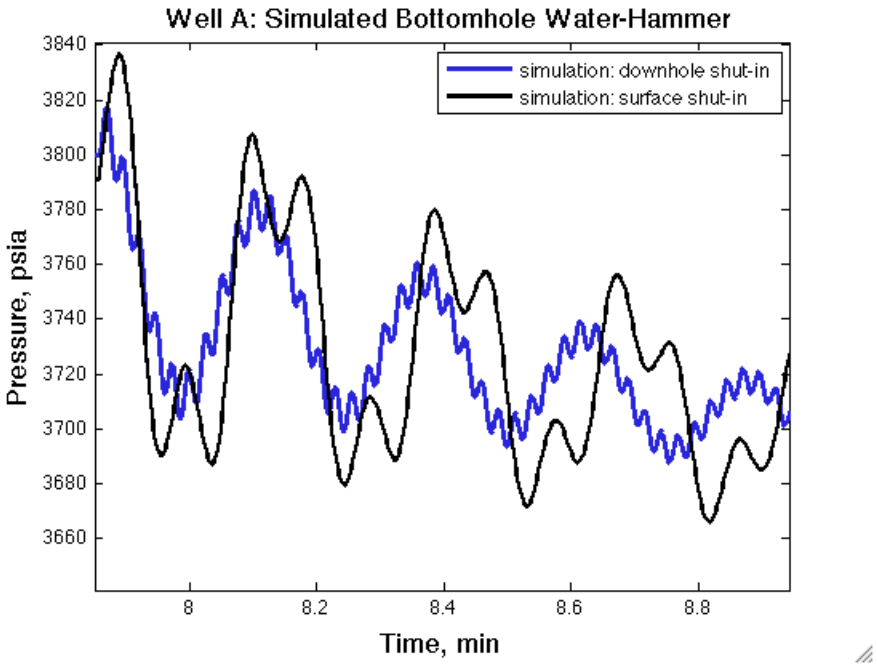

Figure 3.20: Simulated bottomhole water hammer for a downhole shut-in in well A with different formation properties.

3.4 FRACTURE DIAGNOSTICS IN INJECTORS

McCarty and Norman (2006) maintain that the injection pressure gradients in these wells are below the adjusted fracture gradients after taking into consideration the increased pore pressure due to several years of injection. In that case, the model cannot calculate fracture dimensions, as injection pressures lower than the fracture pressures violate the model formulation. However, to demonstrate the capabilities of the model, equivalent fracture dimensions have been calculated by assuming that there exists a 500 psi net-pressure in all the wells, which is not necessarily true. The equivalent fracture dimensions and near wellbore frictional pressure drop calculated from the model parameters have been presented in Table 3.2. It can be seen that the near wellbore frictional pressure drops (representative of the connectivity of the wellbore to the formation) are in good agreement with the observed data. Please also note that these are equivalent fracture dimension as per the assumptions of the model. These injectors are in high permeability formations (~ 1000 to 2000 md) and therefore the resistance, capacitance and inertance are also influenced by the formation as explained in the model formulation.

A portable and easy-to-use tool was also created by implementing this model in Excel VBA. The tool can be used to analyze the effects of different valve closure times, injection rate, well geometry and valve positions, as wells as estimate equivalent fracture dimensions from water hammer data for injectors or minifrac jobs.

3.5 FRACTURE DIAGNOSTICS FROM MINIFRAC DATA

Several minifrac jobs were also analyzed with this tool. The conditions in a minifrac job (a single unpropped fracture and more accurate estimate of minimum horizontal in-situ stress) are closer to the assumptions of the fracture model and make it a better candidate for testing this model. Fig. 3.21 and 3.22 show the comparison of the

modeled and the measured tubing head pressure (THP) data and bottomhole pressure (BHP) data for a minifrac job in an offshore well. The bottomhole pressure data (Fig. 3.22) shown in this case is at the sand face. It can be seen that the model accurately predicts the sand face water hammer magnitude, frequency and waveform. The discrepancy in the decline rate and the few extra cycles in the modeled results are due to the viscoelastic frac fluid being modeled as a Newtonian fluid. The attenuation of the water hammer to tens of psi at the sand face from approximately 1000 psi at the surface should also be noted. This is a confirmation of our simulated attenuation in the injector water hammer cases discussed previously.

The fracture dimensions calculated from the model have been compared to the ones obtained from a commercial simulated in Table 3.3. It can be said that the fracture dimensions are reasonable and comparable.

Fracture Dimensions	**Calculated from Model**	**Calculated from E-Stimplan**
Height (ft)	81.7	75
Half Length (ft)	69.3	35
Width (in)	0.13	0.22

Table 3.3: Comparison of fracture dimensions obtained from model with dimensions from fracture simulator for a minifrac job.

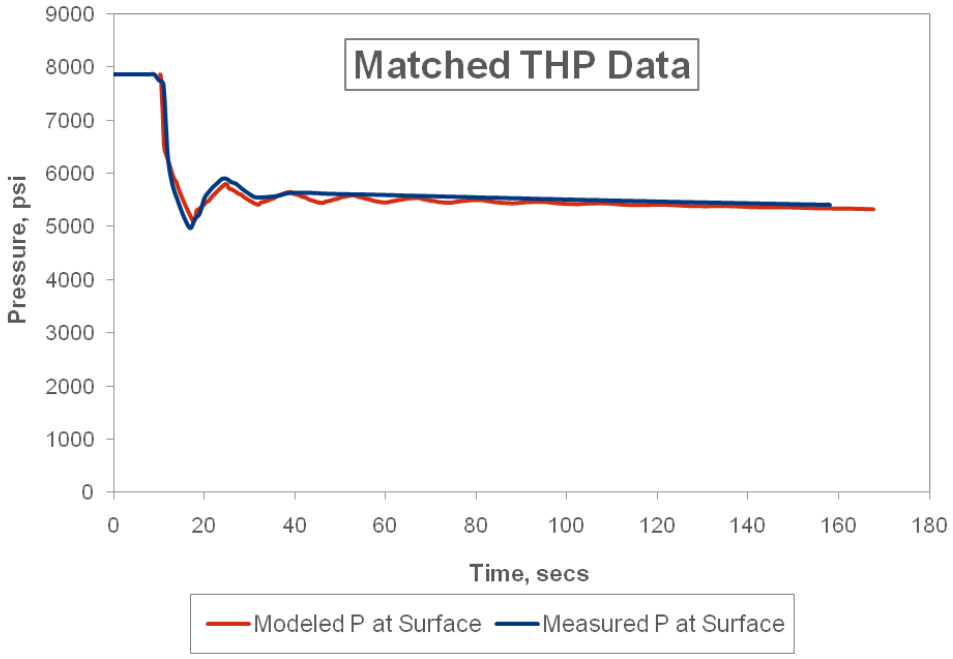

Figure 3.21: Comparison of modeled and measured surface water hammer pressure for a minifrac job.

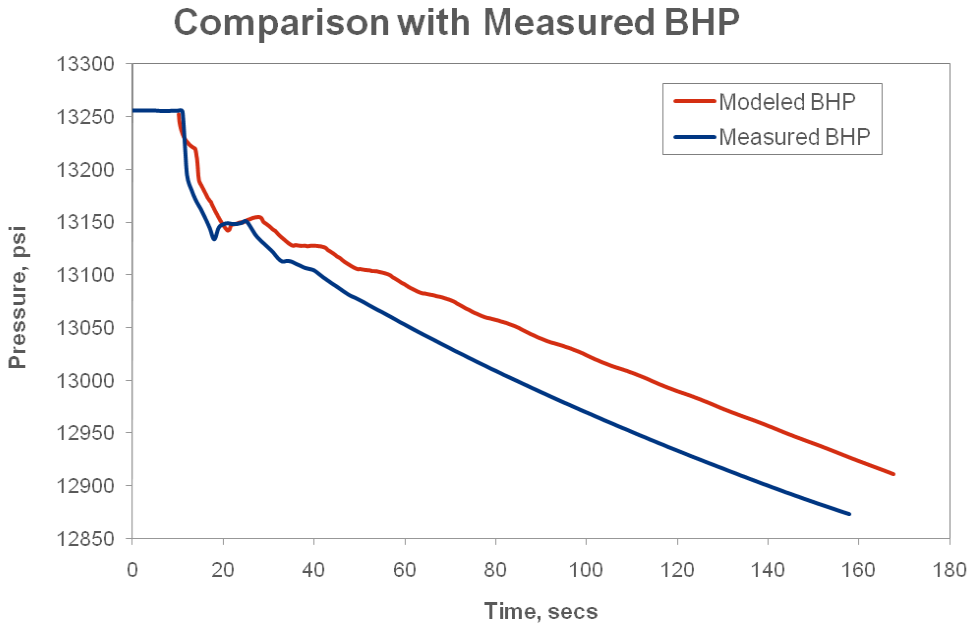

Figure3.22: Comparison of modeled and measured bottomhole water hammer data for a minifrac job.

Chapter 4: Conclusion

A pressure transient is generated when a sudden change in injection rate occurs due to a valve closure or injector shutdown. This pressure transient, referred to as a water hammer, travels down the wellbore, is reflected back and induces a series of pressure pulses on the sand face. The resulting pressure surges can often lead to reduced injectivity, cross flow between zones, sand face failure and sand production. This study presents a semi-analytical model to simulate the magnitude, frequency and duration of water hammer in wellbores, which can be used to understand its impact on wellbore stability in poorly consolidated sands. A *RCI* model has been suggested that can describe the interface, between the wellbore and the formation.

Pressure transients measured in five wells in an offshore field are history matched with the model to obtain typical model parameters. It is shown that the model accurately predicts the effect of injector rate, rate of shutdowns and other well parameters. The implications for completion design and sand control in injectors are discussed.

It is shown that the amplitude of the pressure waves may be up to an order of magnitude smaller at the sand face when compared with surface measurements. This suggests that sand failure may not be as big a concern as originally thought. However, some concerns still remain.

The primary concerns in injectors may be a combination of the following factors. The sand that is already in a failed state due to high rate injection may be liquefied and sucked in to the wellbore due to pressure waves. A transient rate hammer accompanying the pressure hammer may cause fines migration and mobilization, and failure of sand bridges. Cross-flow induced by shut-in between unevenly charged layers can also cause

fines to enter the wellbore. If enough time is not allowed for fines and sand to settle prior to reinjection, plugging of gravel packs and screen can lead to reduced injectivity. Downhole valve closures should be avoided as they create a pressure wave of comparable magnitude but much higher frequency than surface shut-ins, which can potentially cause more damage.

Finally, a model has been proposed to estimate fracture dimensions from water hammer data. The model has been used to obtain equivalent fracture dimensions from injector and minifrac water hammer events. The model shows reasonable agreement with fracture dimensions obtained from commercial simulators.

Appendix

The **complete elliptical integral of the first kind** K is defined as:

$$K(m) = \int_0^{\pi/2} \frac{d\theta}{\sqrt{1 - m^2 \sin^2 \theta}} = \int_0^1 \frac{dt}{\sqrt{(1 - t^2)(1 - m^2 t^2)}}$$

Numerically K can be approximated as

$$K(1 - x) = (c_0 + c_1 x + c_2 x^2) + (d_0 + d_1 x + d_2 x^2) \log(1/x)$$

where, $c_0 = 1.3862944$, $c_1 = 0.1119723$, $c_2 = 0.0725296$, $d_0 = 0.5$, $d_1 = 0.1213478$, $d_2 = 0.0288729$.

The **complete elliptical integral of the second kind** E is defined as:

$$E(m) = \int_0^{\pi/2} \sqrt{1 - m^2 \sin^2 \theta}\, d\theta = \int_0^1 \frac{\sqrt{(1 - m^2 t^2)}}{\sqrt{(1 - t^2)}} dt$$

Numerically E can be approximated as

$$E(1 - x) = (1 + a_1 x + a_2 x^2) + (b_1 x + b_2 x^2) \log(1/x)$$

where, $a_1 = 0.4630151$, $a_2 = 0.2452727$, $b_1 = 0.1077812$, $b_2 = 0.0412496$.

References

Afshar, M.H., Rohani, M. 2008. Water Hammer Simulation by Implicit Method of Characteristics. *International Journal of Pressure Vessels and Piping* **85**: 851-859.

Allievi, L. 1902. General theory of the variable motion of water in pressure conduits. *Annali della Societa` degli Ingegneri ed Architetti Italiani* **17**(5): 285-325 (in Italian). (French translation by Allievi, in Revue de Me´ canique, Paris, 1904) (Discussed by Bergant et al., 2006).

Allievi, L. 1913. Teoria del colpo d'ariete (Theory of water-hammer.). Atti del Collegio degli Ingegneri ed Architetti Italiani, Milan, (in Italian) (Discussed by Bergant et al., 2006).

Ashour, A.I.S. 1994. A Study of Fracture Impedance Method. *Ph.D Dissertation*. The University of Texas at Austin, Austin.

Barr, D.I.H. 1980. The Transition from Laminar to Turbulent Flow. In: *Proc. Instn. Civ. Engrs.,* Part 2 **69**: 555-562.

Bergant, A., Simpson, A.R., Vı´tkovsky´, J. 2001. Developments in Unsteady Pipe Flow Friction Modeling. *Journal of Hydraulic Research* **39**(3): 249-257.

Bergant. A., Simpson, A.R., Tijsseling, A.S. 2006. Water Hammer with Column Separation: A Historical Review. *Journal of Fluids and Structures* **22**: 135-171.

Bergeron, L. 1935. Etude des variations de re´ gime dans les conduites d'eau-Solution graphique ge´ ne´ rale (Study on the Steady-State Variations in Water-Filled Conduits-General Graphical Solution) (in French). *Revue Ge´ ne´ rale de l'Hydraulique* **1**(1): 12-25. (Discussed in Saikia and Sarma, 2006).

Bergeron, L. 1936. Estude des coups de beler dans les conduits, nouvel exose' de la methodegraphique. *La Technique Moderne* **28**: 33. (Discussed in Saikia and Sarma, 2006).

Brunone, B., Golia, U.M., Greco, M. 1991. Modeling of fast transients by numerical methods. In: Proceedings of the International Meeting on Hydraulic Transients with Column Separation. 9th Round Table, IAHR, Valencia, Spain. pp. 215-222.

Chaudhry, H.M., Hussaini, M.Y. 1985. Second-order Accurate Explicit Finite-Difference Schemes for Water Hammer Analysis. *Journal of Fluids Engineering* **107**: 523-529.

Chaudhry, H.M. 1987. Applied Hydraulic Transients. 2nd ed. Van Nostrand Reinhold Company, New York.

Chen, N.H. 1979. An Explicit Equation for Friction Factor in Pipe. *Ind. Eng. Chem. Fund.* **18**: 296.

Ghidaoui, M.S., Mansour, G.S., Zhao, M. 2002. Applicability of Quasi Steady and Axisymmetric Turbulence Models in Water Hammer. *Journal of Hydraulic Engineering* **128**(10): 917-924.

Greyvenstein, G.P. 2006. An Implicit Method for Analysis of Transient Flows in Piping Networks. *International Journal for Numerical Methods in Engineering* **53**: 1127-1148.

Halliwell, A.R. 1963. Velocity of a Water Hammer Wave in an Elastic Pipe. *ASCE Journal of Hydraulic Division* **89**(4): 1-21.

Hayatdavoudi, A. 2006. Well Sanding and Lost Production Due to Cyclic Water Hammer. Paper SPE 100928 presented at SPE Annual Technical Conference and Exhibition, San Antonio, 24-27 September.

Holzhausen, C.R., Gooch, R.P. 1985. Impedance of Hydraulic Fracture: Its Measurement and Use for Estimating Fracture Closure and Dimensions. Paper SPE 13892 presented at SPE/DOE Low Permeability Gas Reservoirs Symposium, Denver, 19-22 May.

Holzhausen, C.R., Egan, H.N. 1986. Fracture Diagnostics in East Texas and Western Colorado using Hydraulic-Impedance Method. Paper SPE 15215 presented at the SPE Unconventional Gas technology Symposium, Louisville, 18-21 May.

Hornaby, B.E., Johnson, D.L., Winker, K.W., Plumb, R.A. 1989. Fracture Evaluation using Reflected Stoneley Wave Arrivals. *Geophysics* **54**(10): 1274-1288.

Joukowsky, N. 1900. On the Hydraulic Hammer in Water Supply Pipes. Me´ moires de l'Acade´ mie Impe´ riale des Sciences de St.-Petersbourg **8**(9): 5 (in German). English translation by, Simin, 1904.

KSB Know-how, Volume 1: Water Hammer. 2006. KSB, www.ksbpak.com/pdfs/waterhammer.pdf/ . Downloaded 10 November 2010.

Khalevin, N.I. 1960. Measurement of rock porosity by sonic well logging. *Razvedochnaya i Promyslovaya Geofizika* **30**: 3-9.

Mathieu, F., Toksoz, M.N. 1984. Application of Full Waveform Acoustic Logging Data to the Estimation of Reservoir Permeability. Proceedings, Soc. of Exploration Geophysicists 54th International Meeting, Atlanta. pp. 9-12.

McCarty, R.A., Norman, W.D. 2006. The Resiliency of Frac-Packed Subsea Injection Wells. Paper SPE 102990 presented at SPE Annual Technical Conference and Exhibition, San Antonio, 24-26 September.

Medlin, W.L. 1991. Fracture Diagnostics with Tube Wave Logs. Paper SPE 22872 presented at the 66th Annual Technical Conference and Exhibition, Dallas, 6-9 October.

Morris, R.L., Grine, D.R., Arkfeld, T.E. 1964. Using Compressing and Sheer Acoustic Amplitudes foe Location of Fracture. Journal of Petroleum Technology 16: 623-632.

Moos, D., Quan, Y. 2006. Methods and Devices for Analyzing and Controlling the Propagation of Waves in a Borehole Generated by Water Hammer. US Patent No. US2006/0293857A1.

Paige, R.W., Murray, I.R., Roberts, J.D.M., Mellor, D.W. 1992. Fracture Measurement using Hydraulic Impedance Testing. Paper SPE 24824 presented at the 68th Annual Technical Conference and Exhibition, Washington, DC, 4-7 October.

Paige, R.W., Murray, L.R., Roberts, J.D.M. 1993. Field Application of Hydraulic Impedance Testing for Fracture Measurement. Paper SPE 26525 presented at the SPE Annual Technical Conference and Exhibition, Houston, 3-6 October.

Parmakian, J. 1963. Water Hammer Analysis. Dover Publications, New York.

Patzek, T.W., De, A. 2000. Lossy Transmission Line Model of Hydrofractured Well Dynamics. *Journal of Petroleum Science and Engineering* **25**(1-2): 59-77.

Saikia, M.D., Sarma, A.K. 2006. Simulation of Water Hammer Flows with Unsteady Friction Factor. *ARPN Journal of Engineering and Applied Sciences* **1**(4): 35-40.

Santarelli, F.J., Skomedal, E., Markestad, P., Berge, H.I., Nasvig, H. 2000. Sand Production on Water Injectors: Just How Bad Can It Get? *SPE Drill. & Compl* **15**(2): 132.

Schönfeld, J.C. 1951. Analogy of Hydraulic, Mechanical, Acoustic and Electrical Systems. *Appl. Sci. Res.* **3**(B): 417-450.

Shimada, M., Okushima, S. 1984. New Numerical Model and Technique for Water Hammer. *Journal of Hydraulic Engineering* **110**(6): 736-748.

Shylapobersky, J., Wong, G.K., Walhaug, W.W. 1988. Overpressure Calibrated Design of Hydraulic Fracture Stimulations. Paper SPE 18194 presented at the 63rd SPE Annual Technical Conference and Exhibition, Houston, 2-5 October.

Silva-Araya, W. 1993. Energy Dissipation in Transient Flow. *Ph.D Dissertation*. Washington State University, Washington.

Silva-Araya, W., Chaudhry, M.F. 1997. Computation of Energy Dissipation in Transient Flow. *Journal of Hydraulic Engineering* **123**(2): 108-115.

Streeter, V.L., Wylie, E.B. 1967. Hydraulic Transients. McGraw Hill, New York.

Tang, X.M., Cheng, C.H. 1989. A Dynamical Model for Fluid Flow in Open Borehole Fractures. *Journal of Geophysical Research* **94**(B6): 7567-7576.

Trikha, A.K. 1975. An Efficient Method for Simulating Frequency-dependent Friction in Transient Liquid Flow. *Journal of Fluids Engineering* **97**: 97-105.

Vardy, A.E., Brown, J.M.B. 2004. Transient Turbulent Friction in Fully Rough Pipe Flows. *Journal of Sound and Vibration* **270**(1-2): 233-257.

Vardy, A.E., Hwang, K. 1991. A Characteristic Model of Transient Friction. *Journal of Hydraulics Research* **29**(5): 669-684.

Vaziri, H., Nouri, A., Hovem, K., Wang, X. 2007. Computation of Sand Production in Water Injectors. Paper SPE 107695 presented at the European Formation Damage Conference, Scheveningen, 30 May-1 June.

Walker, T. 1962. Fracture zones vary acoustic signal amplitudes. *W. O*. **154**(6).

Wang, X., Hovem, K. 2008. Water Hammer Effects on Water Injection Well Performance and Longevity. Paper SPE 112282 presented at the SPE International Symposium and Exhibition on Formation Damage Control, Lafayette, 13-15 February.

Wood, D.J. 2005a. Water Hammer Analysis – Essential and Easy (and Efficient). *Journal of Environmental Engineering* **131**(8): 341-348.

Wood, D.J., Lindireddy, S., Boulos, P.F., Karney, B., McPherson, D.L. 2005b. Numerical Methods for Modeling Transient Flow. *Journal of the American Water Works Association* **97**(7): 104-115.

Wylie, E.B., Streeter, V.L. 1993. Fluid Transients in Systems. Prentice-Hall, New Jersey.

Zhao, M., Ghidaoui, M.S. 2003. Efficient Quasi Two Dimensional Model for Water Hammer Problems. *Journal of Hydraulic Engineering* **1129**(12): 1007-1013.

Zhao, M., Ghidaoui, M.S. 2004. Godunov-type Solutions for Water Hammer Flows. *Journal of Hydraulic Engineering* **130**(4):341-348.

Zielke, W. 1968. Frequency-dependent Friction in Transient Pipe Flow. *Journal of Basic Eng, ASME.* **90**(9): 109-115.